DOCUMENT NO:	EFRC – ABS01 (3)	FAA PROJECT NO:	
CURRENT REVISION:	IR	INITIAL DATE:	11/15/10

Status Report 1

EVALUATION OF RESIDUAL STRENGTH OF BEECHCRAFT BONANZA SPAR CARRY-THROUGH WITH FATIGUE CRACKS

Conducted for the
AMERICAN BONANZA SOCIETY

DEPARTMENT: Embry-Riddle Aeronautical University - Eagle Flight Research Center

SECTION: Technical Analysis

PREPARED BY: Snorri Gudmundsson

TECHNICAL APPROVAL:

PREPARED BY:

MANAGER APPROVAL: Richard P. Anderson

REVISION APPROVAL

REV	REVISED BY	APPROVED BY	DATE	REV	REVISED BY	APPROVED BY	DATE
IR	SG	RPA	11/15/10				
1							
2							
3							

REVISION HISTORY

Revision	DESCRIPTION OF CHANGE
-	

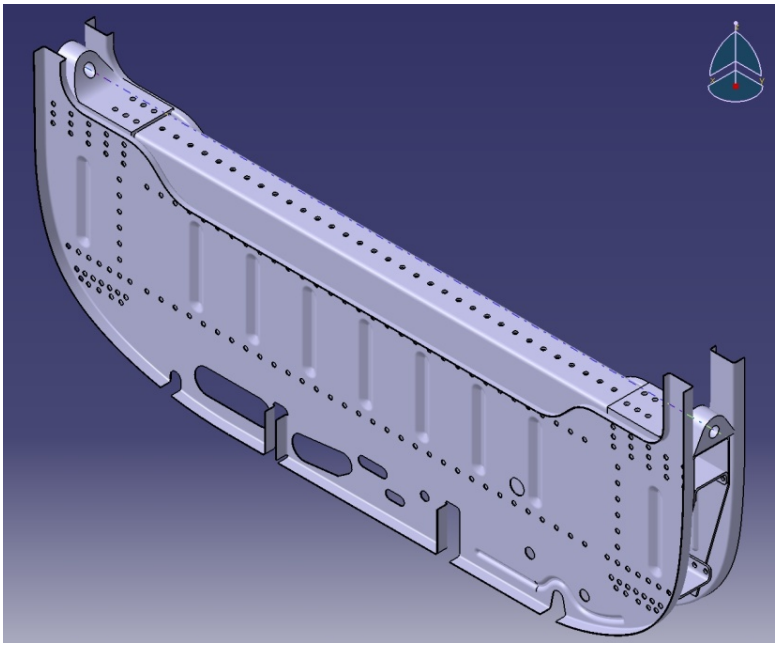

Principal Investigator:	Snorri Gudmundsson Assistant Professor of Aerospace Engineering Embry-Riddle Aeronautical University
Prepared by:	Snorri Gudmundsson
Research team supervisor:	Dr. Eric Hill

Research Team (alphabetical order by last name):
Lori Costello, Christopher Foti, Harshad Lalan, Ning Leung, Andrea Palacios, Zachary Sager, Michael Scheppa, Isadora Thisted

EMBRY-RIDDLE AERONAUTICAL UNIVERSITY

Table of Contents

EVALUATION OF RESIDUAL STRENGTH OF BEECHCRAFT BONANZA SPAR CARRY-THROUGH WITH FATIGUE CRACKS

1. INTRODUCTION

This is the first of three status reports considered the deliverables in an investigation currently being conducted by Embry-Riddle Aeronautical University (ERAU) research faculty on behalf of the American Bonanza Society (ABS). The investigation is performed in accordance with ERAU Research Project 13776 (signed on 9/22/2010) and an agreement between ERAU and ABS presented in a Statement of Work (SOW).

The prologue to this project is the appearance of fatigue cracks in the main spar carry-through structure of selected types of Beechcraft aircraft. The cracks appear only in specific versions of those airplanes (ones whose shear web thickness is 0.040"[1]) and whose estimated operational cycles to failure range from 2400 to 14,000 cycles, or approximately 3-4000 flight hours[2]. A survey of the cracks indicates a greater incidence of forward versus aft web cracking (4:1)[3]. Their formation has lead to the issue of Mandatory Service Bulletins (MSB) by Beechcraft and Airworthiness Directives (AD) by the FAA (see References 1-4).

The detection of these cracks dates back to 1980s[4] and the issued MSBs (References 3 and 4) affects selected versions of the Baron, Travel Air, Model 35 Bonanzas, Model 33 Debonairs/Bonanzas through 1985 models and all Model 36 Bonanzas through 1985 models[5]. The MSBs require the carry-through area to be inspected after 1500 flight hours, and then every 500 or 200 subsequent flight hours depending on whether or not cracks have been detected. The MSB that applies specifically to the Bonanza aircraft can be seen in Reference 4. Additionally, Beechcraft designed a special "repair kit" in an attempt to remedy the situation, but it has gained notoriety in the field for being difficult to install.

ERAU was contracted in September 2010 to investigate the residual strength of the main spar carry-through in Beechcraft Bonanza aircraft. Initially ERAU provided ABS with a Research Plan to assess costs and manpower required. This plan can be seen in Appendix A of this document. The plan split the project into 3 separate phases, each focusing on a specific aspect of the investigation. The first two comprise the research; the last phase is the presentation of conclusions in a final report. An important aspect of the agreement is that both ABS and ERAU can opt out if it is determined the projected results will not yield useful information for ABS. This report covers Phase I, whose subtasks are listed in Appendix B.

The scope of the project has been defined in teleconferences with ABS and the FAA ACO in Wichita, Kansas. A consensus on the scope has been achieved, which limits it to the determination of residual

[1] See note with Slide 2 of Reference 12.
[2] See Slide 37 of Reference 12.
[3] See Slide 37 of Reference 12.
[4] See note with Slide 2 in Reference 13.
[5] See Slide 2 in Reference 13 and Reference 4 for full effectivity of the MSB.

strength in the spar carry-through assembly at ultimate load with selected lengths and locations of cracks, and not causal mechanism. This well defined scope narrows the approach to a standard "certification-style" fail-safe structural analysis, which usually means the evaluation of *Geometry->Loads->Stress->Margin of Safety*. This, in turn, means that only certification loads need to be determined. The first two, Geometry and Loads, are addressed in this status report.

Since this document is the first of three status reports, its findings are not conclusive. It is simply an update provided to ABS to explain progress made to date. It is expected that both ABS and the FAA be given the opportunity to review and address its shortcomings. In accordance with industry protocols it is considered the "Initial Release" (Revision IR) and ERAU will release a subsequent "Revision A" if deemed necessary[6], either prior to *Status Report for Phase II* or by incorporating responses into that document. The author hereby requests and welcomes comments and suggestions for improvements.

The history of crack growth in Bonanza aircraft is well documented in References 6-11 and need not be repeated here. The cited documents include technical evaluations by several consultants and the perspectives of FAA officials. A disparity of views regarding the cause and severity of the cracks is apparent from these documents. This project is not intended to take a stand for or against any of the views expressed or, as stated earlier, to investigate the cause of the crack formation. Instead its sole intent is to evaluate the impact of the discrepancy on the continued airworthiness of the affected aircraft. The Principal Investigator, who has no stake in the outcome, has reviewed the cited references and found each side to offer some sound arguments; however, his ultimate goal is an unbiased approach.

Note that the Bonanza was certified to Civil Air Regulations 3 (CAR 3). A limited discussion of differences between CAR 3 and the present day equivalent CFR 14, Part 23 is provided in Appendix F.

2. ABS' PERSPECTIVE

ABS's position on the crack growth issue is clearly stated on Slide 11 of Reference 12 and Slide 30 of Reference 13, here paraphrased for clarity:

- At this time (2009[7]) the issue has been known for some 20 years.
- "*Service histories suggest, at least to date, current AD requirements are satisfactorily detecting and addressing cracks, and preventing virtually all growth and/or recurrence of spar web cracking except in very few, unusual cases.*"
- To date there is no known in-flight failure or mishap attributed to spar web cracking of any of these aircraft.
- ABS asked the FAA for time to investigate the issue to assess the urgency of the required repair, which is notoriously hard to implement.

3. FAA's PERSPECTIVE

FAA's current position is stated in a letter to Mr. Tom Turner dated January 25, 2010 (Reference 14 and reproduced in Appendix E). Among items the FAA requested are added load cases and a matrix of crack

[6] This will be done "free of charge" to ABS provided the resulting workload isn't prohibitive.
[7] 2009 is when the PowerPoint presentation was compiled.

lengths on both the front and rear shear webs. The matrix of requested crack scenarios is applicable to Phase II analysis and will be brought up for discussion in future teleconferences, should ABS decide the ERAU research should continue into Phase II.

4. PROJECT PROCESS

The ultimate goal of the project is to evaluate the residual strength of the spar carry-through structure with fatigue cracks present. Strictly speaking there appear to be two ways to evaluate this. The first is a sort of a brute force way, in which a representative airplane that features a prominent crack formation is loaded to failure to determine the ultimate load it can react. The second approach is analytical. Both approaches have their pros and cons. For instance, if we ignore the prohibitive cost of the first approach, the question inevitably becomes one of applicability. In other words, if the ultimate load is known for a particular crack geometry, is it applicable to another airplane with a different crack geometry? The drawback of the second approach is assurance of accuracy in modeling the discrepancy. Its primary advantage is far less cost and far more crack geometries and load scenarios can be considered. This is the path that has been chosen.

In short, the research team intends to use the Finite Element Method (FEM) to evaluate the residual strength in the assembly. In this approach, one of the first tasks is the digitization of the carry-through structure into a solid modeler. This has already been accomplished using the state of the art solid modeler CATIA. This electronic representation will be converted into a NASTRAN Finite Element (FE) model, which will be validated by comparing strains between the actual structure and the FE model under identical test loads. If necessary, the FE model will be refined to better match actual strains. Finally, the FE model will be loaded with reaction loads based on load analysis based on CAR 3.

Step	Description	Phase
1	Collect information about the geometry of the structure.	I
2	Collect information about the materials used in the structure.	II
3	Determine certification or requested loads reacted by the structure.	I
4	Construct a FE model of the structure.	II
5	Validate the FE model by applying specific loads to the original structure (which will be instrumented) and evaluate its prediction accuracy.	II
6	Determine stresses and strains in the structure resulting from the reaction of loads.	II
7	Determine if these exceed material allowables.	II

5. GEOMETRY

The spar carry-through structure (see Figure 1) was digitized using a combination of measurements made using a FARO arm digitization equipment and direct measurements with calipers. More details about the process can be found in Appendix F.

The information extracted, in turn, was used to create a solid model in CATIA (see Figure 2). Figure 3 shows one of the many important benefits of using this approach. CATIA allows the user to better understand the nature of the load paths by permitting parts of the assembly to be partially or fully removed to reveal internal details of the structure. Figure 3 shows clearly the internal C-channels that form the spar caps and the shear panels forming the shear web. The second major benefit is that the method allows the solid model to be imported into a FE solver like NASTRAN for further analysis. Among other benefits is the ability to measure or confirm distances in hard to reach places.

A collection of images of the model can be found in Appendix C.

6. ACCURACY OF MEASURED GEOMETRY

The project has been hampered by the lack of participation by Hawker Beechcraft. It is important for the reader to be mindful of this serious drawback that precluded the research team from accessing "official" technical drawings. This leaves no option but to reverse-engineer parts using images and drawings that are in the public domain. A possible consequence of this is dimensional errors that can creep in, although the research team strives to minimize them by cross-checking dimensions. This situation was partially remedied by Mr. Tom Turner of the ABS, who graciously shipped an entire spar carry-through assembly, salvaged from a "retired" Bonanza, for the research team. This allowed the team to extract important dimensions with high accuracy (see Figure 1). A large part of the work presented in here would not have been possible had it not been for this gesture. Figures 2 and 3 show the spar carry-through structure once it was modeled in the solid modeler CATIA.

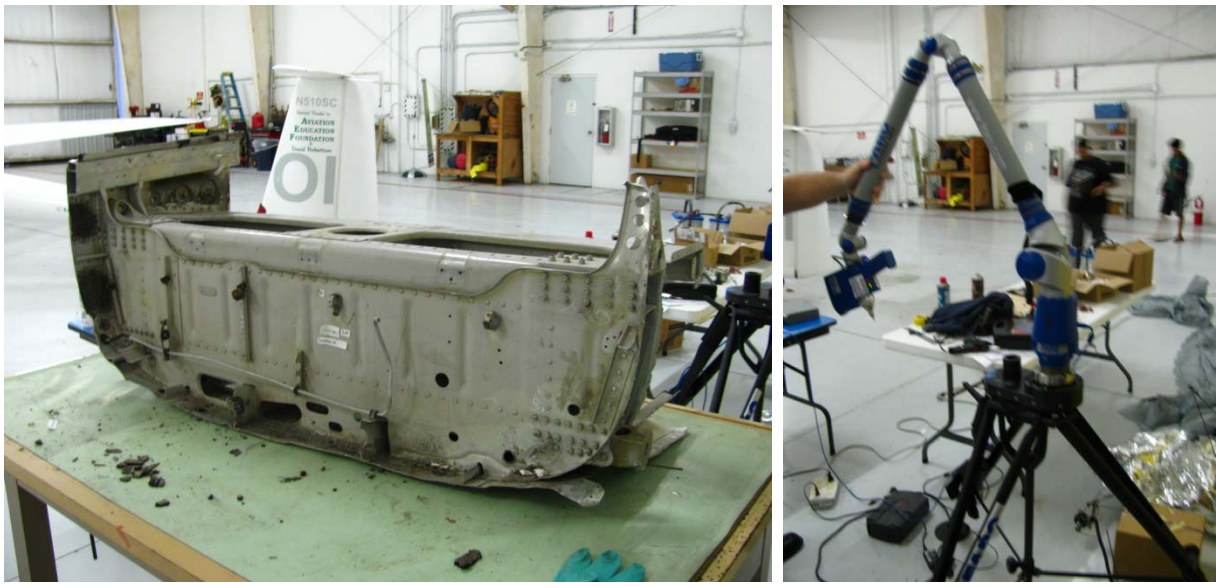

Figure 1: Spar carry-through assembly and the FARO arm.

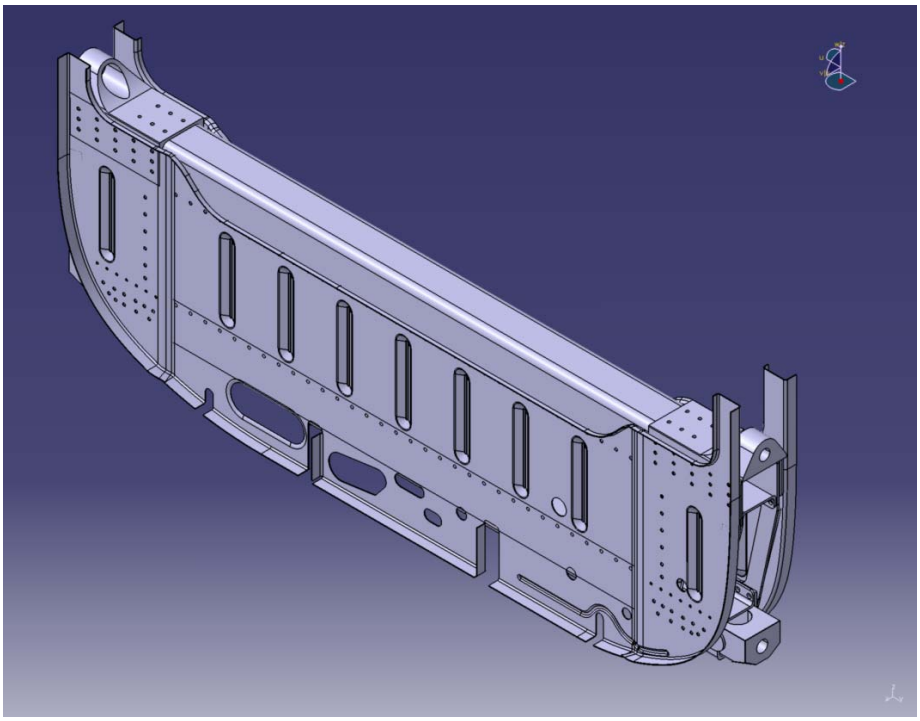

Figure 2: A CATIA isometric representation of the assembly.

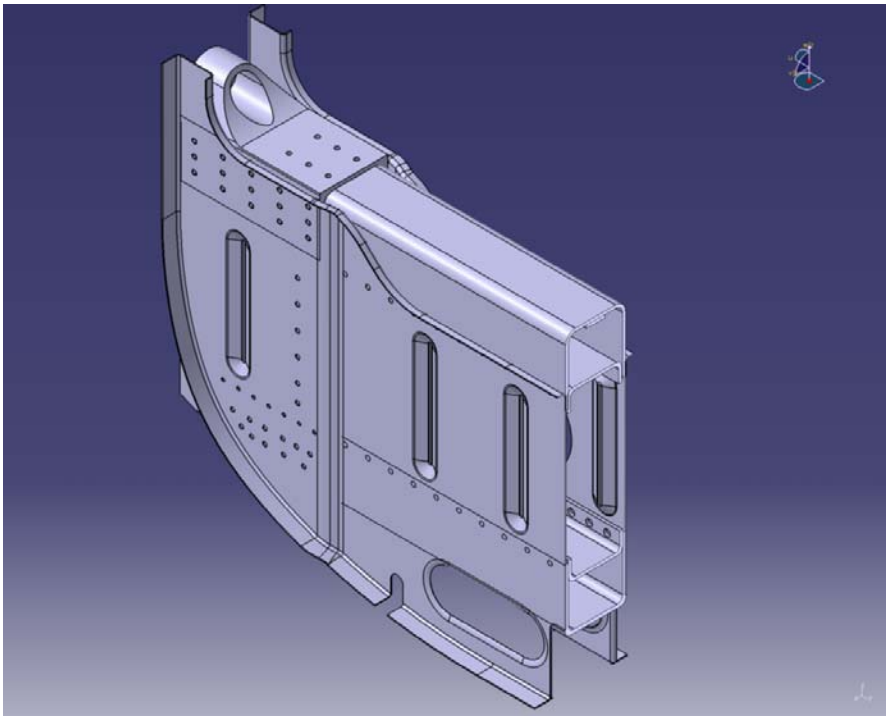

Figure 3: The spar carry-through assembly cut-away reveals the box-type spar cap design of the Bonanza aircraft.

The accuracy of the FARO arm is of the order of ±0.001". Calipers are perhaps ±0.005". Measurements based on drawings are much less accurate. It must be recognized that the limited access to external geometric features inevitably introduces slight error in the analysis. There are typically two kinds of error that may creep in; a *direct measurement error* and *image distortion error*. Direct measurement error can be quantitatively exemplified by considering the wing area and the resulting wing loading of the Beech Bonanza wing. Data published by Beechcraft specifies the wing span of the A36 Bonanza as 33.5 ft, wing area of 181 ft^2, and certified the gross weight of 3600 lb_f. These numbers mean that the wing's average chord is 181 ft^2/33.5 ft = 5.40 ft and the wing loading at gross weight is 3600 lb_f /181 ft^2 = 19.89 lb_f/ft^2. As an example, consider the three-view drawing in Figure 4. A scaled up version of this figure was used to estimate the Outside Mold Line (OML) using the computer software CATIA and SURFACES (see Section 11) to do the scaling. Now, say we measure the wing span and chord from the three-view drawing in Figure 4 in a manner that introduces an error of -1 inch to each parameter. Therefore, one could possibly measure the wing span as 33.5-0.083 = 33.42 ft and the average chord as 5.40-0.083 = 5.32 ft. The resulting wing area would amount to 33.42 ft x 5.32 ft = 177.7 ft^2, which is an error of 1.8%. This means the calculated wing loading will then amount to 3600 lb_f /177.7 ft^2 = 20.26 lb_f/ft^2, also an increase by 1.8% (conservative difference). For this reason, one should expect there to be some error, say ±2%, in all such measurements. The research team assumes an accuracy of ±1 inches when extracting geometric data from such images. In the experience of this author an error of this magnitude is acceptable.

An image distortion error can be caused by a digital image that for some reason may have been "stretched". As a consequence this could make 1 ft measured along the x-axis longer or shorter than if measured along the y-axis. In other words, the image has been made "fat" or "skinny."

7. WORK COMPLETED

(1) Digitization of the spar carry-through structure has been completed (Appendix C).
(2) Evaluation of the airplane's flight loads has been completed (Appendix F).
(3) Evaluation of the airplane's landing loads has been completed (Appendix F).

8. CURRENT STATUS

All the Phase I tasks listed in the Research Plan of Appendix B have been completed. Should ABS decide to continue with the project, it is possible some load cases will have to be refined or added in order to comply with the wishes of the FAA expressed in Reference 14 (see Section 3). This will not add any cost or require changes made to the current agreement between ERAU and ABS.

9. LOADS – METHODOLOGY

The loads presented in this document were developed based on CAR 3 and were developed using the following methodology:

Step	Description	Comment
1	Flight Envelope (aka V-n Diagram)	Generated for the A36 and aerobatic F33C aircraft.
2	Identify extremes	Maneuvering speed V_A and dive speed V_D were identified as the most critical extremes of the envelope. Maximum gust load at the design cruising speed turned out to be less than the g-loading required by the Utility and Aerobatic CAR 3 classification of the airplanes.
3	Construct a Vortex-Lattice Model	A vortex-lattice model was created of the Bonanza using the symbolic vortex-lattice solver SURFACES. The model dimensions were based on scaling up the three-view drawing of Figure 4. A validation samples for the code are provided in Appendix D.
4	Determine air loads	Forces acting on each panel on the wing are summed up (integrated) to calculate the total bending moment and shear at the attachment points.
5	Utilization of loads	These loads will be applied to the FE model during Phase II.

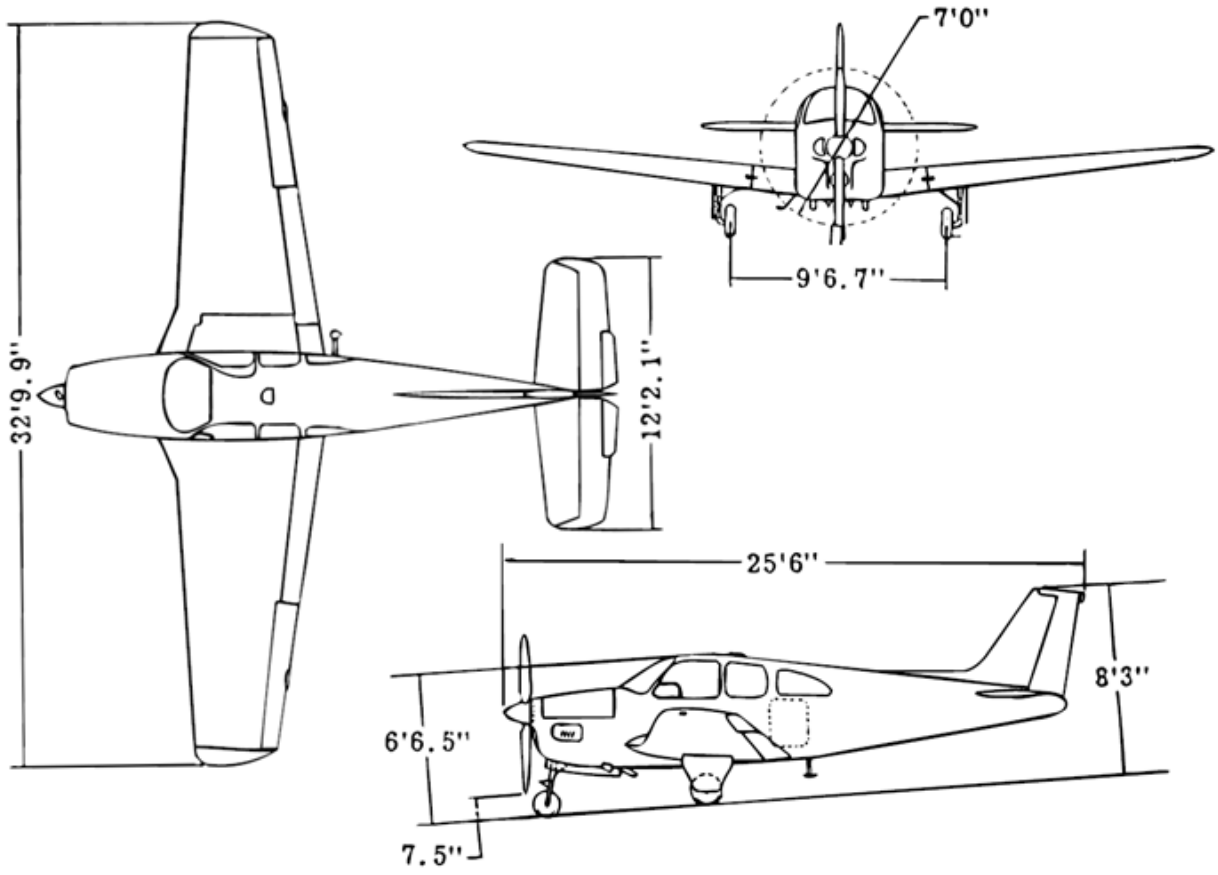

Figure 4: A three-view drawing of the Beech F33C Bonanza.

10. LOADS - FLIGHT ENVELOPE (V-n DIAGRAM)

Flight envelopes have been generated for both airplane types and match the data on the Type Certificate Data Sheet (TCDS). Gust lines were developed using the 3D lift curve slope of the aircraft ($C_{L\alpha}$ = 4.78 per radian[8]) and generate less loads than the envelope shown in Figures 5 and 6.

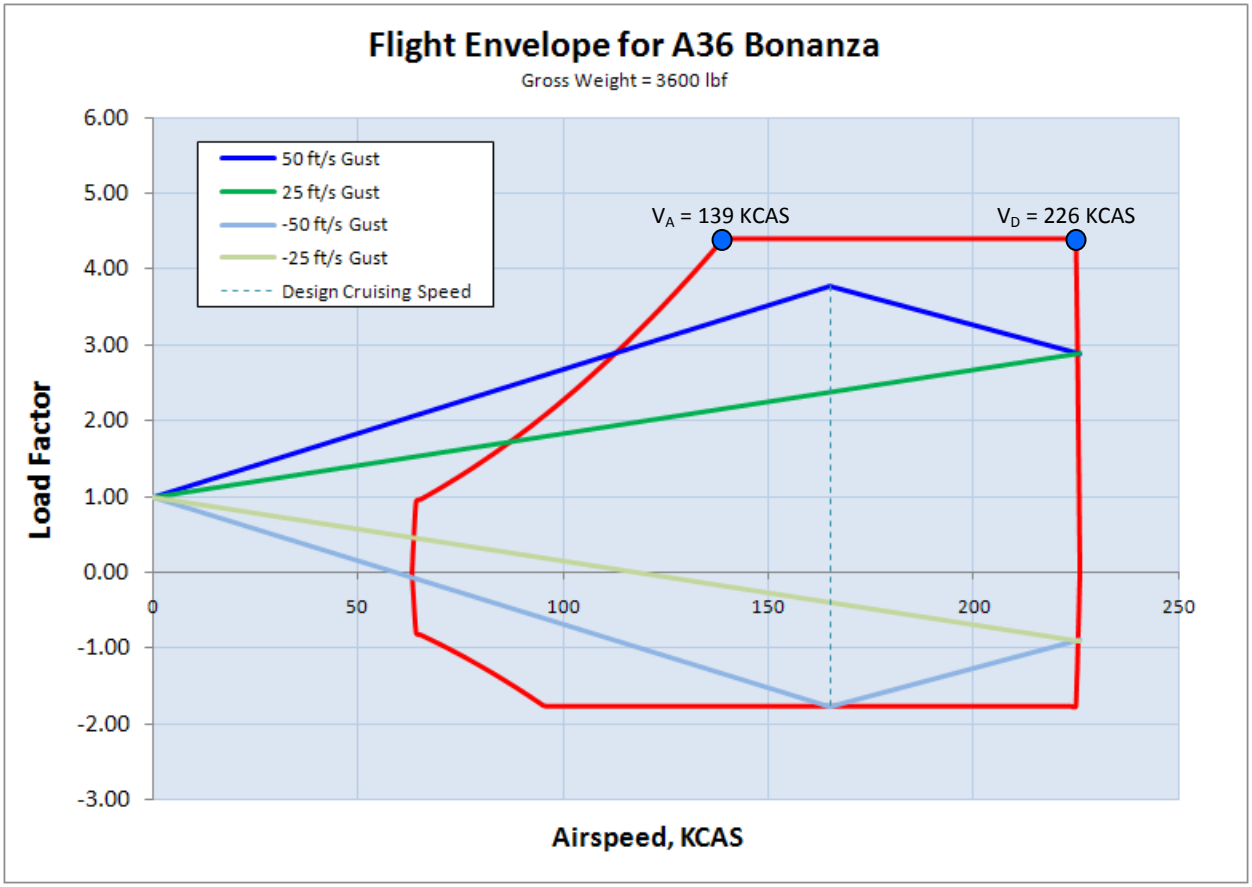

Figure 5: A V-n Diagram for the Beech A36 Bonanza.

[8] Generated using the software SURFACES, see Section 11.

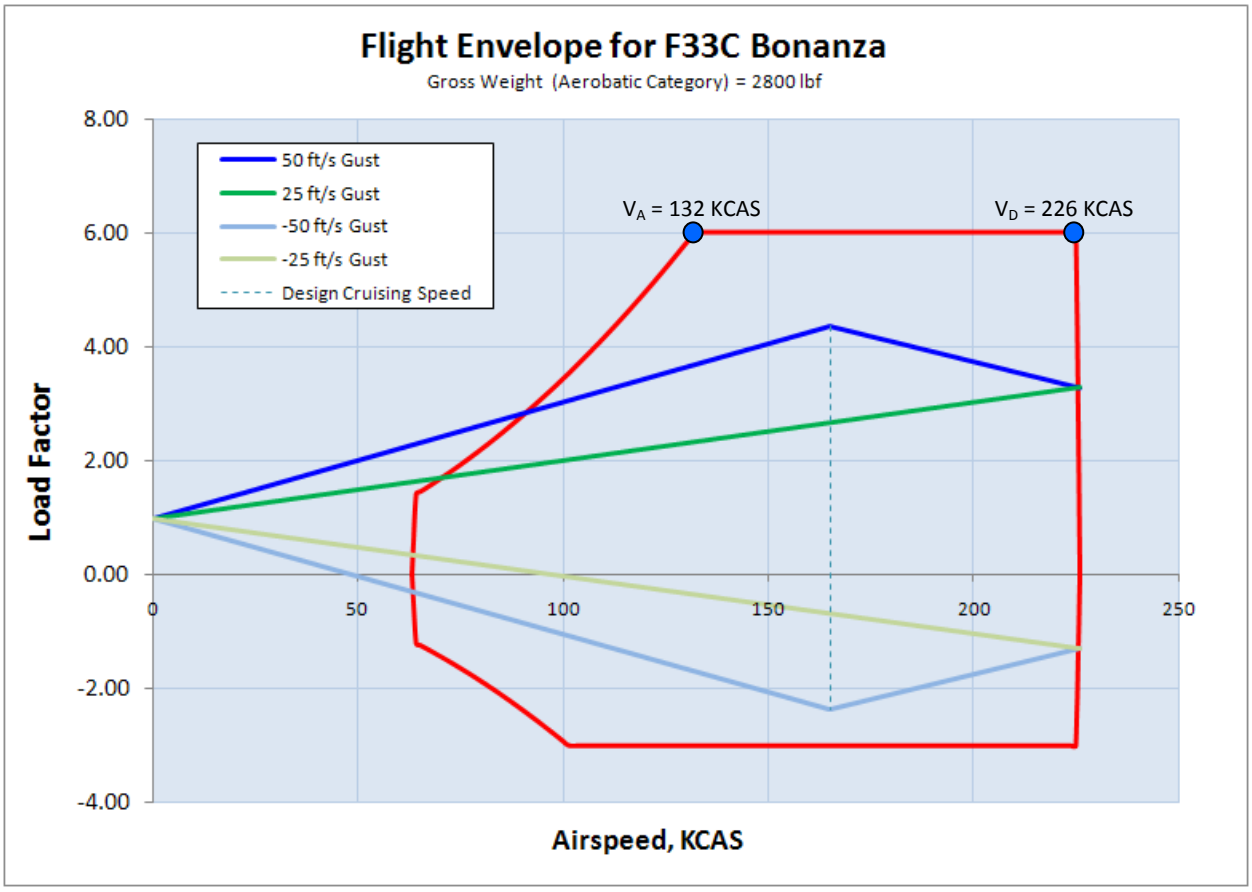

Figure 6: A V-n Diagram for the Beech F33C Bonanza.

11. LOADS – GENERATION OF AIRLOADS

Aerodynamic loads (or airloads) reacted by the wings of the Bonanza were estimated using the *Vortex-Lattice Method* (VLM). VLM is a mathematical method that allows the user to represent an airplane with thin mathematical panels. The method uses these panels to predict the 3D flow field in which the airplane flies. Much can be learned about the aircraft from such predictions, including drag, stability and control parameters, and aerodynamic loads, which are used to size material thicknesses in the airframe.

The details of the method are beyond the scope of this report. The method has been an industry stalwart for over 40 years and has been used in the design of airplanes ranging from the Concorde, F-4, F-14, F-15, down to the simplest ultra light aircraft. In modern times, tools such as Reynolds Averaged Navier Stokes (RANS) software[9] have become increasingly popular in the aircraft industry. However, when comes to turnaround time they are still far behind VLM codes. As an example, at the time of this writing, it takes an experienced CFD person 1-2 weeks, perhaps even more, to create an electronic version of an airplane, depending on complexity. Once the model is ready it is fed into a special program called a "solver". The solver calculates local airspeeds around the airplane, ultimately allowing the operator to extract similar parameters from the solution as that obtained with VLM. The calculations

[9] Also called CFD for Computational Fluid Dynamics. Strictly speaking, VLM is also a CFD method.

can easily take anywhere from 12 to 48 hours, depending on available computer resources. Each solution corresponds to a single airspeed, Angle-of-Attack (AOA) and Angle-of-Yaw (AOY). During the design process multiple such solutions are needed. The author has worked on airplane designs that took 80+ hours to solve using a cluster of 32 computers. In contrast, an experienced user of VLM software can create an airplane model on a desktop or laptop computer in a few hours, and each solution takes 1 to 3 minutes to generate and, if the airflow is smooth ("attached") will give the user exactly the numbers obtained from the RANS solver.

As alluded to earlier, VLM is a very accurate as long as the airflow is not separated. Unlike RANS solvers, VLM solvers work on the premise that the airflow is inviscid (no flow separation can occur). If the actual airflow is separated (due to high values of AOA or AOY) VLM predicts forces that are larger than they would be in reality. For this reason, if VLM is used to calculate wing loads at the maneuvering speed (which is stall speed at limit load) the loads are conservative. The importance of using such a method to calculate the loads can be seen by considering the complications the leading edge extension of the Bonanza wing near the fuselage (strake) introduces to the spanwise distribution of lift. The larger size of the wing in this area lowers the local section lift coefficients, in turn, moving the center of lift outboard. As a consequence, the wing bending moments are slightly higher than they would be without it; an effect that would be very hard indeed to account for without computational fluid dynamics methods. Additionally, on the real aircraft the fuselage and horizontal tail can contribute as much as 5-10% of the total lift, depending on airplane geometry. This effect is accounted for by creating those features on the model of the Bonanza used for the analysis.

The code used for this project is a commercially available VLM code called SURFACES. The author has used this software to analyze many different types of aircraft with very satisfactory results. As an example, it was used extensively by the author during the design of the Cirrus Aircraft SF50 Vision jet. Validation samples have been provided in Appendix E.

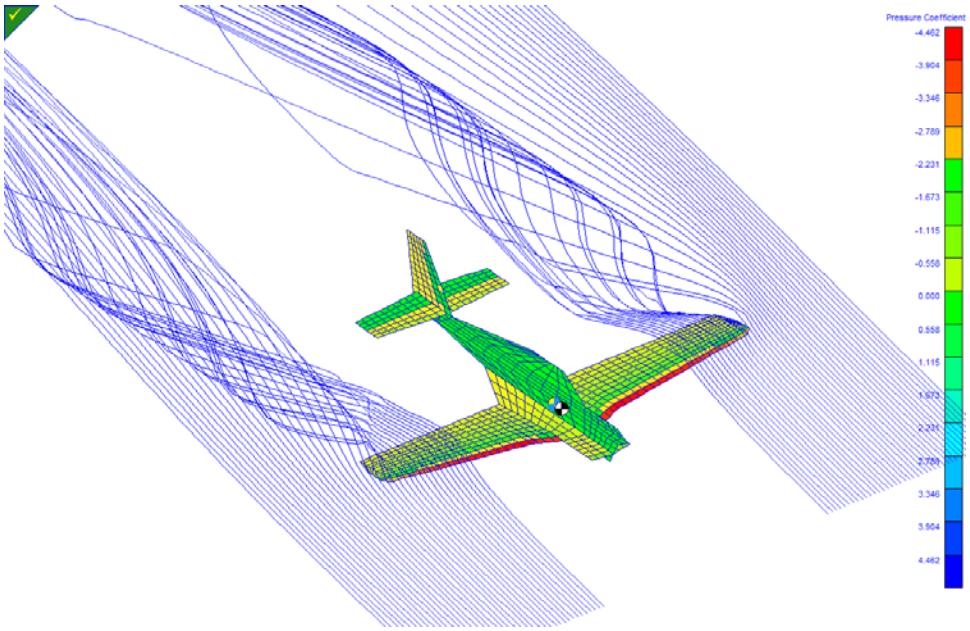

Figure 7: A VLM model of the Beech A36 Bonanza, showing the generation of wing tip vortices.

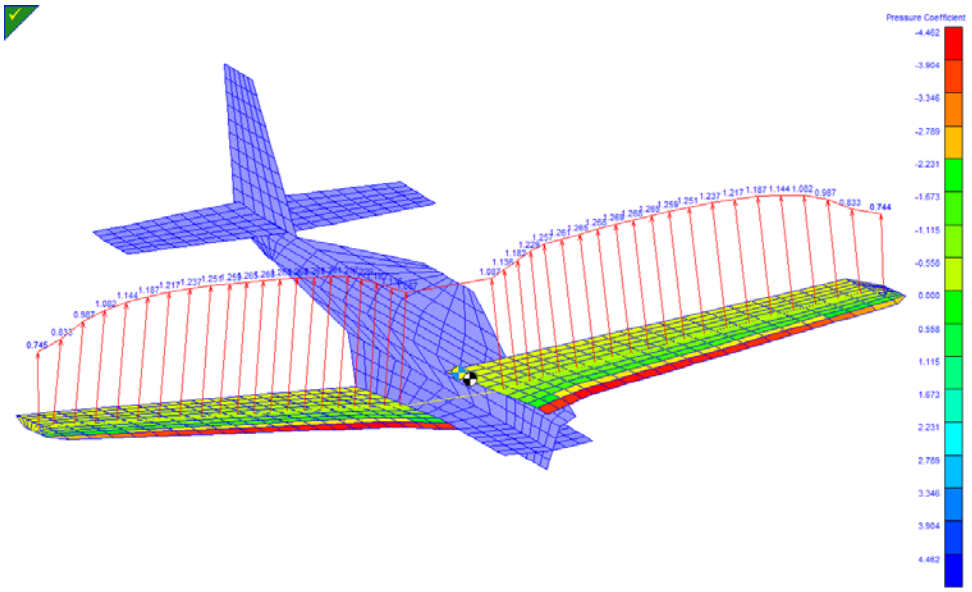

Figure 8: A VLM model of the Beech A36 Bonanza, showing the distribution of lift along its wings as section lift coefficients. The model features the NACA 23016.5 (root) and NACA 23012 (tip) airfoils, as used in the real airplane.

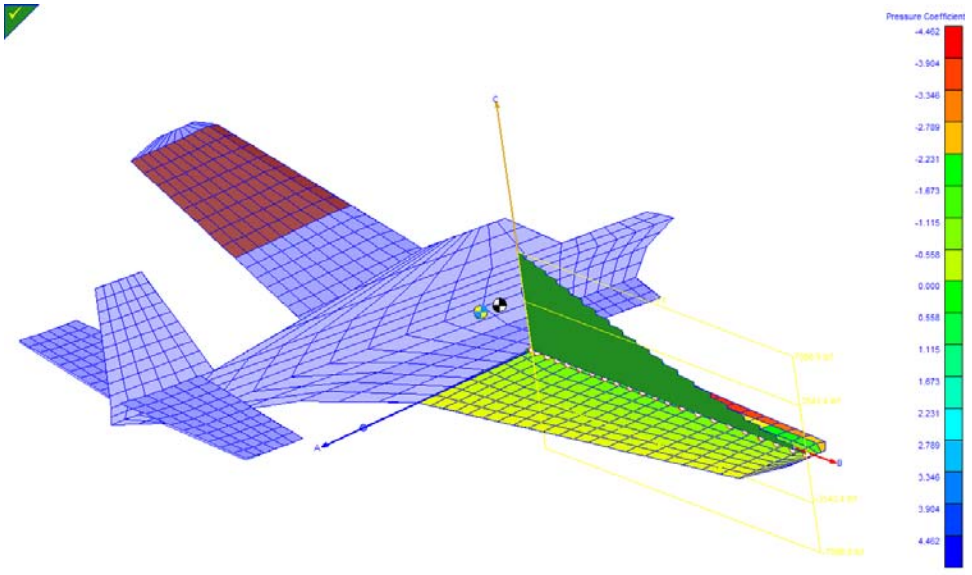

Figure 9: A VLM model of the Beech A36 Bonanza, showing the distribution of shear forces along the wing (shear diagram). The steps in the shear distribution result from discretization of the wing into strips.

12. LOADS – PRELIMINARY LOAD PATH ANALYSIS

Upon request, two models of the Bonanza are considered in this report; the A36 Bonanza (utility category) and F33C Bonanza (aerobatic category). It is of interest to compare their characteristics from a standpoint of aviation regulations[10]. Let's compare these two aircraft types:

Parameter	Symbol	A36 Bonanza	F33C Bonanza
Wing area	S	181 ft²	181 ft²
Wing span	B	33.5 ft	33.5 ft
Spanwise location of the Mean Geometric Chord	y_{MGC}	8.22 ft	8.22 ft
Design gross weight	W_0	3600	2800
Limit load factor	n	4.4g	6.0g
Ultimate load factor	n_{ult}	6.6g	9.0g
Inertia load at ultimate load factor	$n_{ult} \cdot W_0$	23760 lb_f	25200 lb_f
Load per wing[11]	F_{wing}	11880 lb_f	12600 lb_f
Landing load factor	n_{ldg}	3.0g	3.0g
Inertia load at ultimate load factor	$n_{ldg} \cdot W_0$	10800 lb_f	8400 lb_f
Load per main landing gear leg	$0.5 \cdot n_{ldg} \cdot W_0$	5600 lb_f	4200 lb_f

This simple analysis shows that of the two the F33C reacts higher ultimate flight loads, whereas the landing loads for the A36 are higher (see the shaded cells in the table). Let's ponder this further by building simple models for 2D Finite Element Analysis and simple. The analysis that follows is performed with the 2D FE analysis software Beam Analyzer. The analysis is only intended to give a rough idea of the reaction loads and average stresses in the shear panel and spar cap on a macroscopic scale. It is not a substitute for the 3D FEA being prepared for Phase II and remains to be supported by experiment (e.g. by strain gauging the actual web). The load transferred through the spar caps into the shear web and the fuselage skin in the actual structure is a complicated phenomenon and requires a more sophisticated modeling. The 2D analysis omits microscopic effects of stress concentration caused by the huck-bolt fastener pattern, as well as that of crack geometry. It also ignores the inertia effect of the fuselage, which is transferred through the rivets to the flange of the shear web. Having addressed those shortcomings, the reader may be wondering why do it at all? Well, the fact is that simple analyses not only give important clues about where to place strain gauges for FE model validation, they reveal in no uncertain terms where the load paths lie. The importance of understanding the load paths is fundamental to the greater understanding of how the loads are reacted by the structure. Additionally, this will provide the ABS and the FAA with numerical free-body diagrams to refer to in future discussions and teleconferences.

Let's first provide shear and moment diagrams for the symmetric and asymmetric flight load cases.

The simple model in Figure 10 represents an idealized version of the wing and spar carry-through structure. The reader should note that in reality this force is distributed along the wing, but it can be idealized as a point load (12600 lb_f) acting at a specific distance (spanwise location of the MGC = 75.58 in) outboard from the attachment point. This will result in the same shear force and moment as reacted

[10] These airplanes were certified using the now obsolete CAR 3.

[11] Here incorrectly assuming each wing carries the entire half load (i.e. fuselage and horizontal tail contributions are ignored).

by the wing attachments due to the distributed wing load. It is only a mathematical simplification. The model consists of 3 beam elements. The left and right beams transfer the wing lift to the carry-through (center beam) and extend to the spanwise location of the Mean Geometric Chord (MGC). This configuration guarantees that both shear and moment will be reacted by the carry-through and allows us to calculate the shear and moment diagrams for two important load cases; ultimate symmetrical and ultimate asymmetrical flight loads (see CASEs 1 and 2 later in this section). These two important diagrams can be seen in Figures 11 and 12. Note that the model is constrained in two locations. Node 2 is a simple support (fixed x- and y- location, but rotation is allowed). Node 3 is a sliding constraint that only restricts displacement along the y-axis.

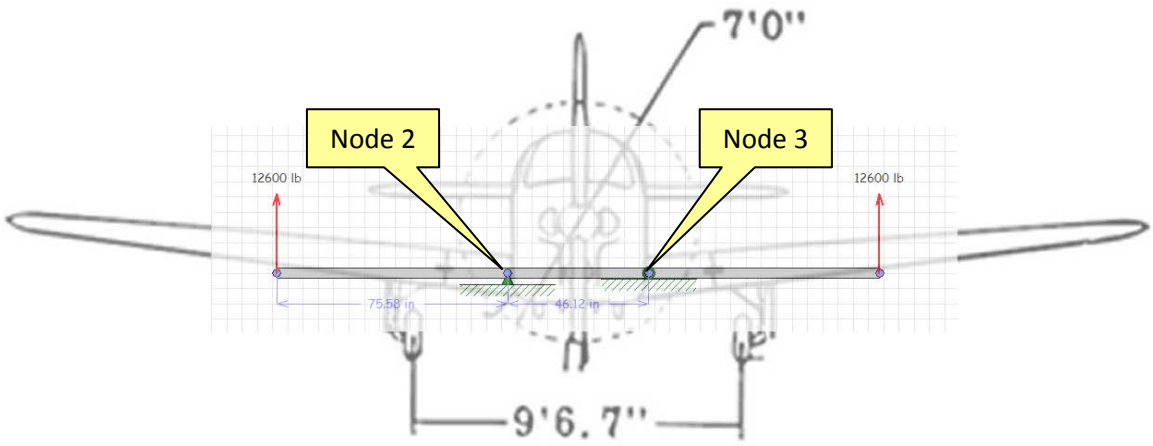

Figure 10: A simple 2D FE model representing the wing and spar carry-through.

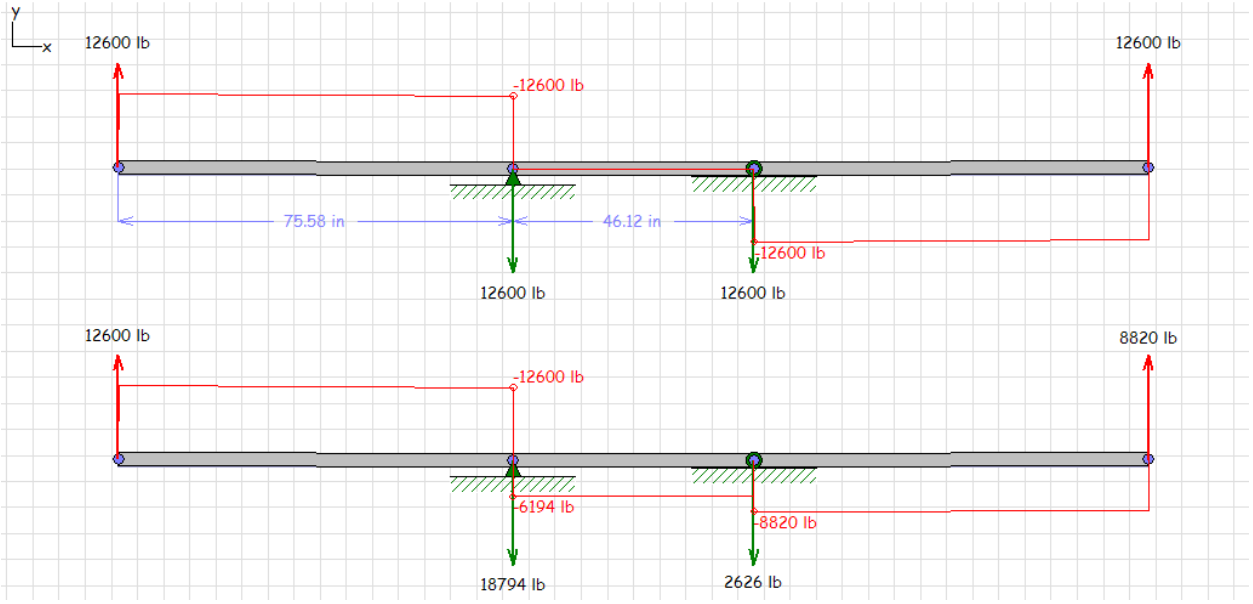

Figure 11: A shear diagram for CASE 1 and CASE 2. Note that no shear is transferred through the carry-through in the symmetrical case (it is reacted as fastener shear and bending moments). Substantial shear (comparatively) is transferred in the asymmetrical case.

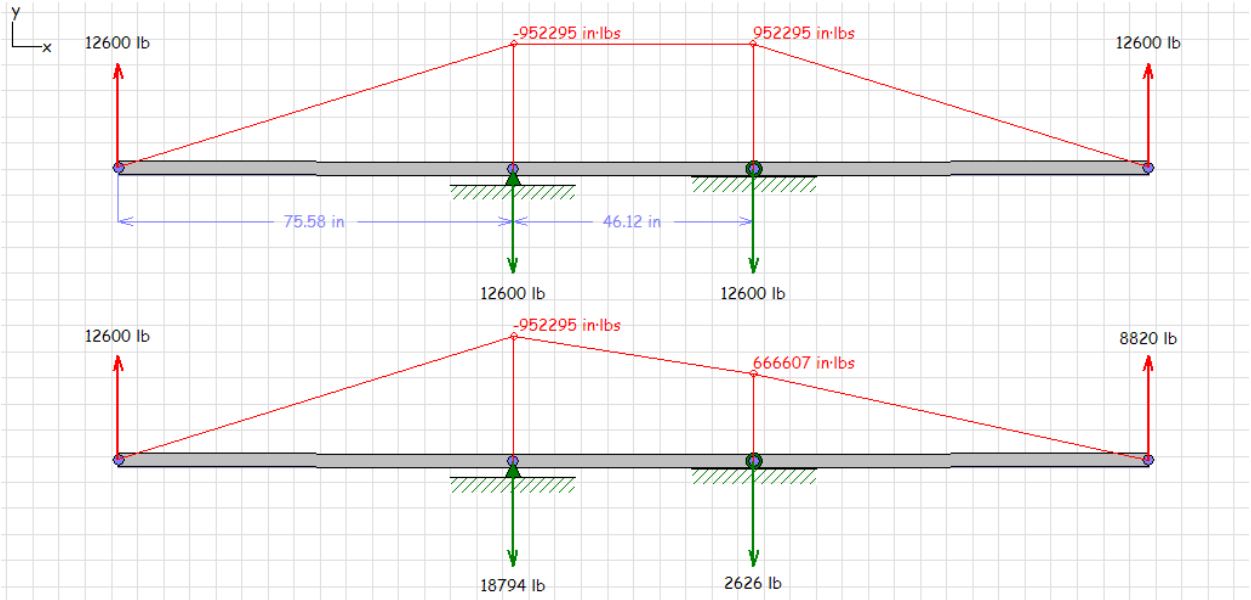

Figure 12: A moment diagram for CASE 1 and CASE 2.

Now, keeping these diagrams in mind, it is prudent to consider what is happening at the carry-through. The model in Figure 13 represents a more complicated version of the one in Figure 10. It features the wing and spar carry-through structure (box in the middle) and is made from 8 rod elements[12] and a single shear panel[13]. The two triangular trusses transfer the wing lift to the carry-through, exactly as done in the previous model. This configuration guarantees that both shear and moment will be reacted by the carry-through as a couple at the wing attachment fasteners.

Note that it doesn't matter that these rods form a triangle and not a parallelogram; it is the reaction forces at the attachments we are interested in and these will be exactly the same for either configuration. The lack of dihedral does not affect the results either for the same reason. The moment transferred to the carry-through amounts to the lift force (12600 lb_f) acting at the spanwise location of the MGC (75.58 inches, which, by the way, is really the reason why we bother to calculate it in the first place) and is a commonly used simplification. The use of rod elements rather than beam elements for the wing truss ensures that loads are transferred to the carry-through as forces, suppressing any moments. This assumption is based on the 7/8 inch diameter wing attachment bolts only transferring shear and axial loads and not moments in the real airplane.

[12] Rod elements only transfer axial loads, whereas beam elements transfer axial and shear loads, in addition to moments.

[13] Shear panels in the finite element method can only react shear.

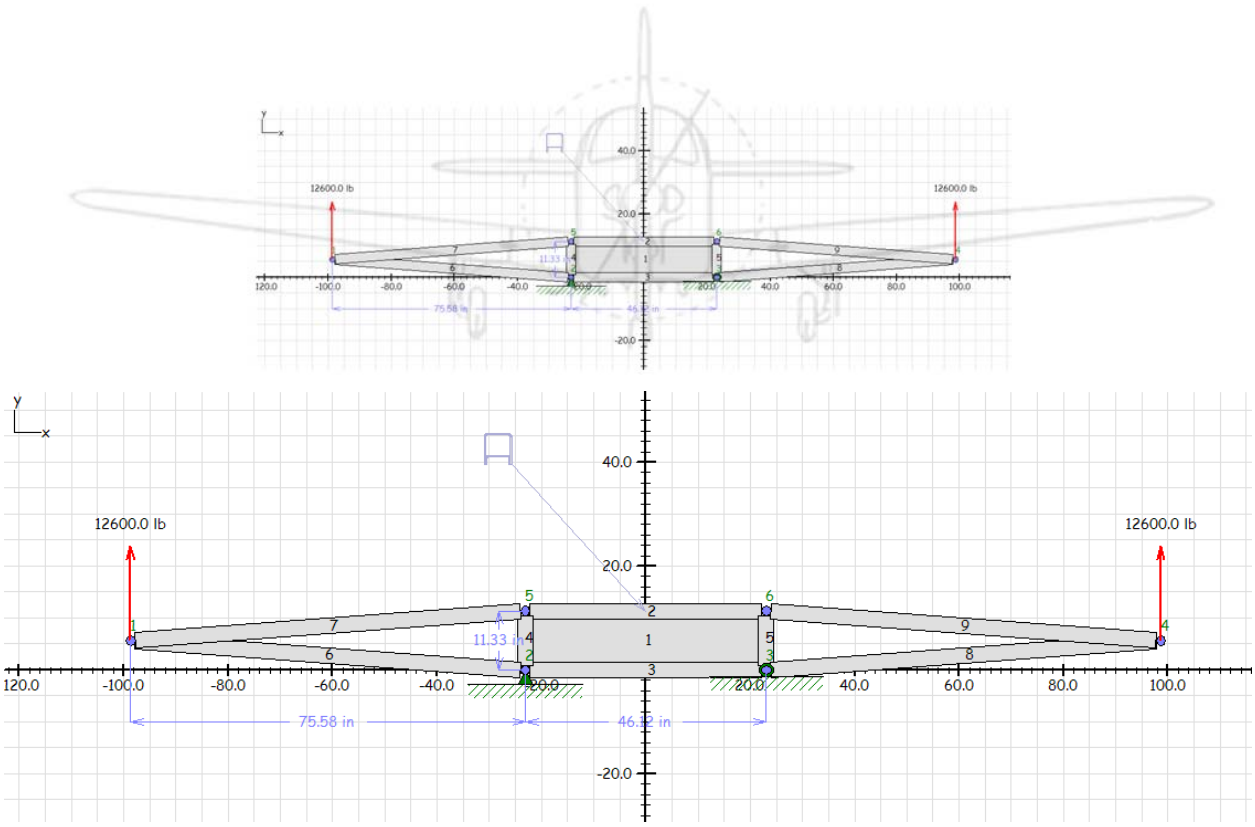

Figure 13: A simple 2D FE model representing the wing and spar carry-through.

The spar carry-through consists of four rod elements that represent the spar caps and the tie plates (vertical rods). These enclose a shear web represented by a shear element of 0.040" thickness, just like the one in the affected Bonanzas. Rod elements are used to ensure that any asymmetric load[14] (refer to Figure 12) transferred through the wing attachment is fully reacted by the shear panel and not as a beam bending moment. This configuration will therefore result in shear stresses in the shear web that are higher than the real airplane will experience. This difference is reacted by the shear element because the rod elements don't react bending moments. In other words, was not for the shear panel, the structure (i.e. the FE model) would collapse when asymmetric loads are applied. This configuration allows us to answer the question what is the largest shear that can possibly form in the panel. The geometric properties of the upper and lower spar caps are based on the actual cross section obtained from the actual spar carry-through (see Sections 4 and 5). It can be seen as the gray cross section to the top and just left of the vertical axis. The cross sectional area of the tie plates is 0.04" x 3" and there are two of those assumed on each side of the carry-through.

With all this said, let's study a few load cases and calculate the magnitude of loads in this representation. For clarity, the IDs of all nodes and elements visible in Figure 13 have been turned off.

[14] For instance, during a yawing maneuver each wing will generate different bending moments. As a consequence, the reaction load transferred through the wing attachment bolts will be different between the two sides of the airplane.

CASE 1: SYMMETRICAL LOAD (12600 lbf) ON EACH WING

This represents the airloads at V_A or V_D, during which the airplane reacts 9g ultimate load. The resulting loads can be seen in Figure 14. The image shows that the shear web is entirely unloaded. The spar caps react 84080 lb_f axial load in tension (red) and compression (blue). The force in the tie plates amounts to 6300 lb_f each.

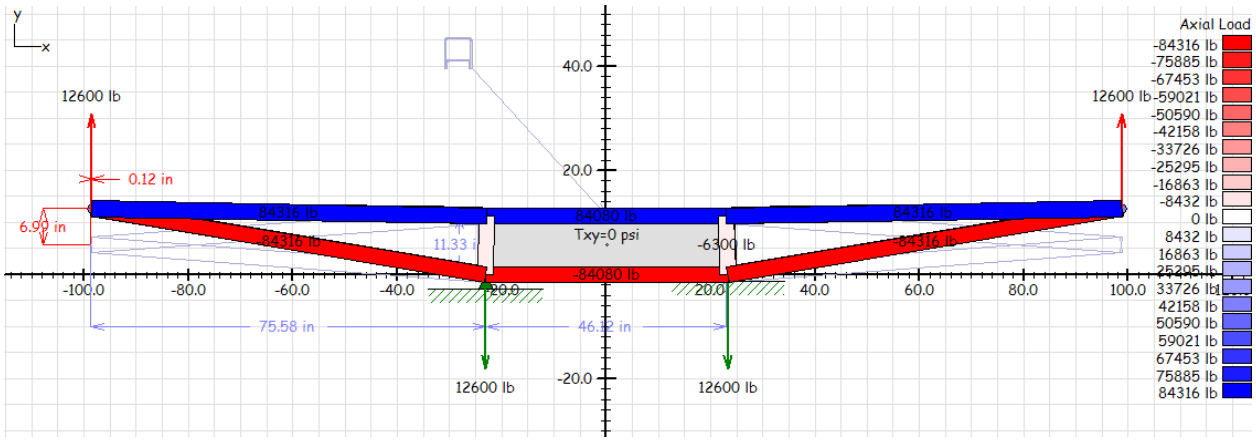

Figure 14: Result for a symmetrical load at 9gs.

CASE 2: ASYMMETRICAL LOAD CASE 100/70

This represents the airloads at V_A during which the airplane reacts 9g ultimate load in a yawed condition. This assumes one wing to react the full 12600 lb_f and the other 70% of that or 8820 lb_f. The resulting loads can be seen in Figure 15. The image shows that although not zero, the shear stress in the shear web is very low or only 181 psi. The spar caps react 71468 lb_f axial load in tension and compression. And the classical scenario of one side of the wing attachment bolts reacting much greater force than the other one is clearly evident. The tension force in the tie plates amounts to 1313 lb_f and 9397 lb_f. This indicates the tie plates "pick up" this load, leaving the shear web more or less unloaded.

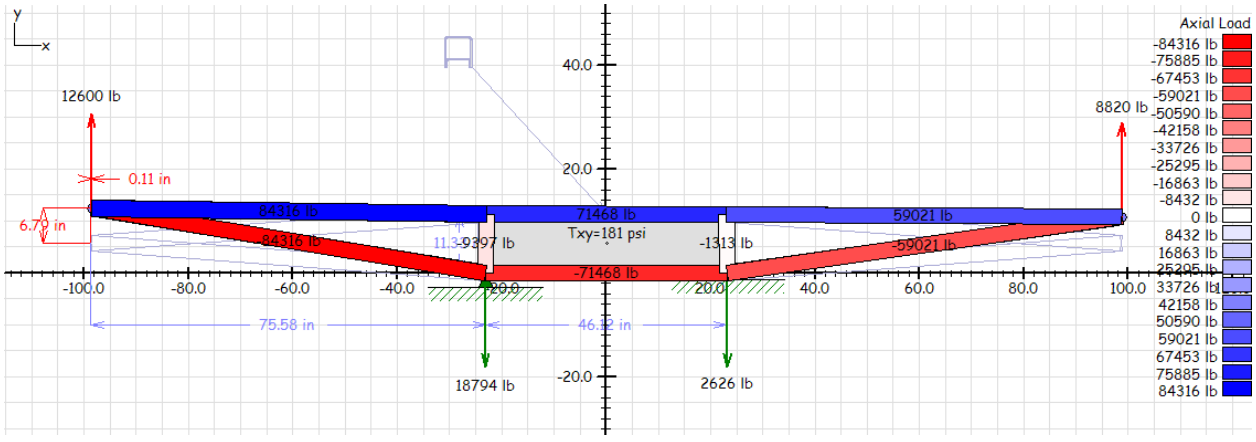

Figure 15: Result for asymmetrical load at 9gs.

CASE 3: SYMMETRICAL TOUCH-DOWN ON MAIN GEAR ONLY.

The model in Figure 13 was further modified to incorporate the main landing gear legs so that reactions due to a hard landing could be evaluated. This model can be seen in Figure 16 with applied forces consisting of a total wing lift of 3600 lb_f (1g lift load) and vertical impact force of 5400 lb_f per CAR 3.243. The magnitude of this force is based on an assumed 3g landing impact (so 3 x 3600 = 10800 lb_f; divide by 2 to get 5400 lb_f). Now, again it is important to remind the reader that the "legitimacy" of these loads is not the main issue, since this exercise is only to develop an expectation for what magnitude of loads is to be expected in the carry-through.

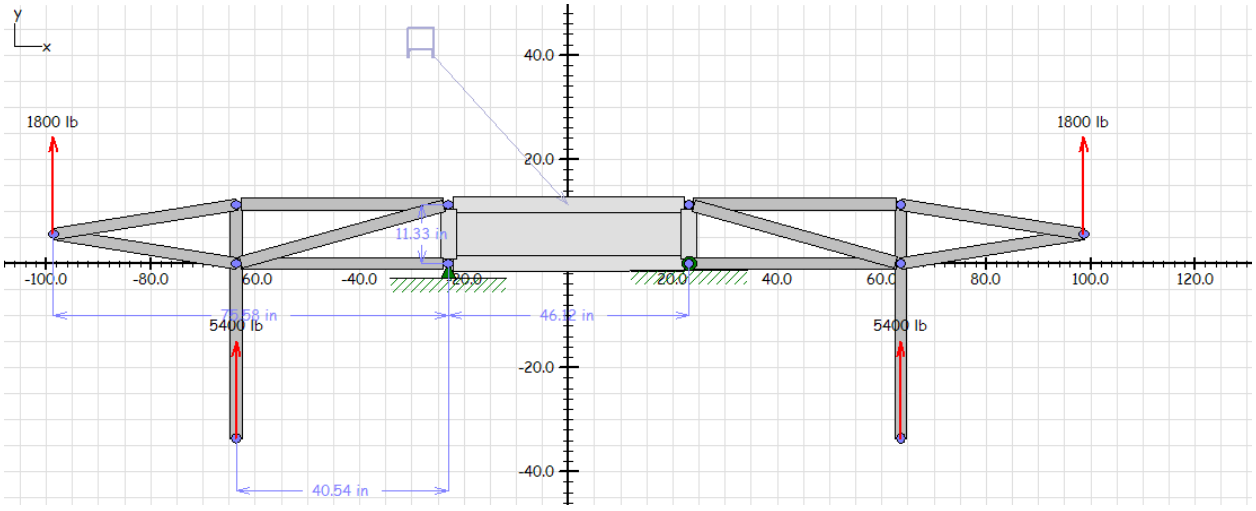

Figure 16: A simple FE model to evaluate the impact of a hard landing on the carry-through.

The results can be seen in Figure 17. Again, the reaction of these forces does not load up the shear web. Also note that the axial loads in the spar caps are less than for either CASE 1 or CASE 2.

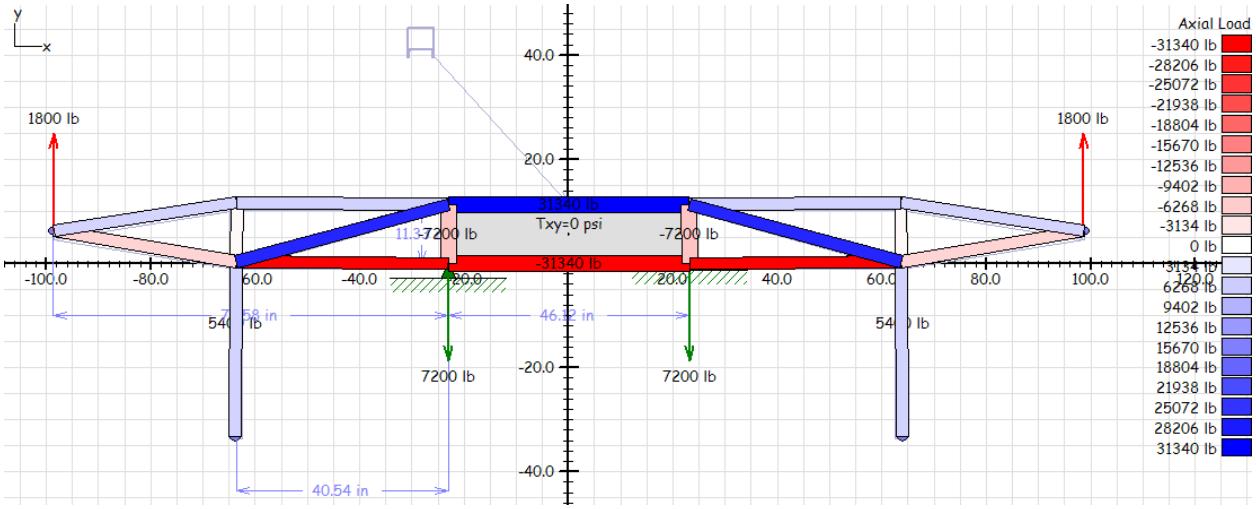

Figure 17: Resulting load diagram for CASE 3.

CASE 4: ASYMMETRICAL TOUCH-DOWN ON MAIN GEAR ONLY.

This severe case assumes the pilot makes a 3g landing on one main gear only. The applied loads are as shown in Figure 18 and the resulting load diagram is shown in Figure 19. It can be seen that again the shear web remains lightly loaded, with an average shear stress of 278 psi, while the tie-plate loads transfers some 17346 lb_f between the two spar caps.

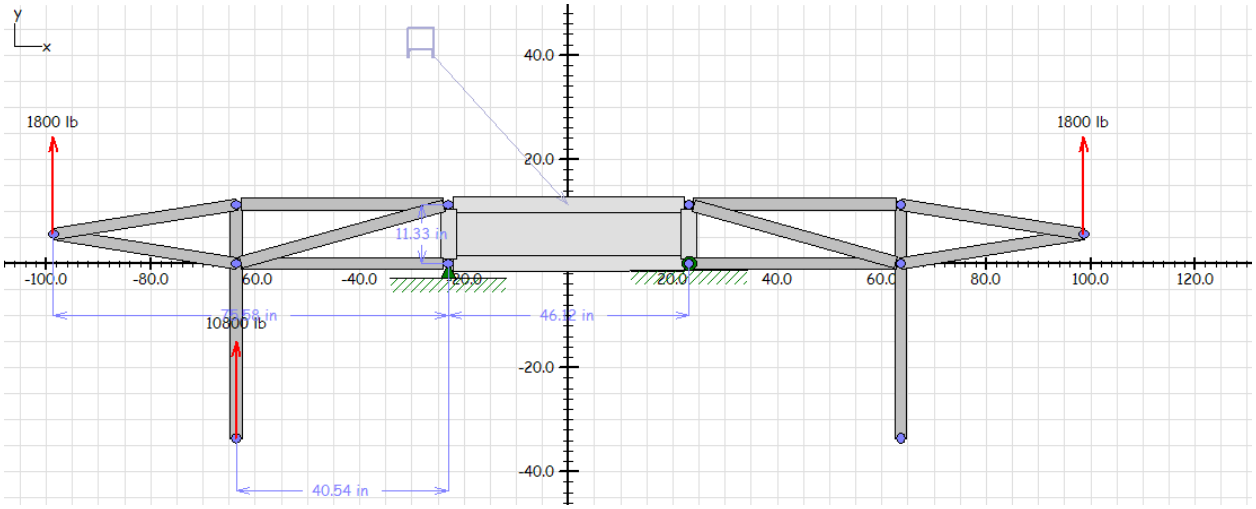

Figure 18: The simple FE model loaded to represent a hard touch-down on one main gear only.

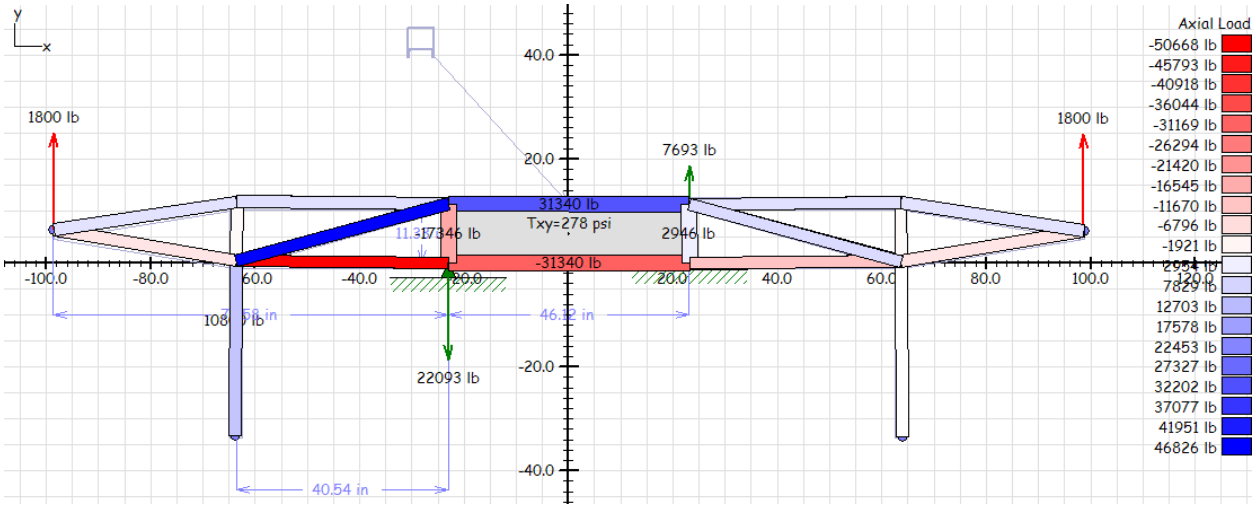

Figure 19: Resulting load diagram for CASE 4.

As stated earlier these studies represent preliminary findings, and should the project continue an attempt will be made to load up the structure and measure strains with strain gages. That effort will either support or reject these results.

13. FUTURE TASKS

- Fail-safe residual strength analysis of the web with the crack lengths and shapes as recommended by the FAA in Reference 15. Perform analysis using ultimate loads.
- Classification of structural elements in the spar carry-through as primary or secondary.
- Confirmation of 2024-T3 as a structural material.
- Load path analysis in the spar carry-through.
- Strain-gage the shear web to demonstrate if the predicted loads are supported by evidence.
- Analyze residual strength of the web with the lower part of the carry-through removed when doing the 3D FE work. This is based on a report written by Mr. Dick Wilson (see Reference 9) and will demonstrate whether this part can be considered primary or secondary structure.

14. FINAL COMMENTS

The analysis of Section 12 begs the question, if the shear web is so lightly loaded, why is it there in the first place? The answer is impossible to know, unless the structural designers can be located and asked or their documentation reviewed. This may be hard to do since the airplane was designed many decades ago. What appears certain is that the *aft* shear web is all but useless in transferring shear loads due to the large openings in it, leaving only the front shear web available for that task. One can surmise that if the structural designers were concerned about large shear loads in the web, perhaps both sides of the carry-through would have been used. However, this is not the case. One possible answer can be that the shear web is there to stabilize the upper cap and prevent it from buckling in compression. A simple buckling check reveals that the compressive load of 84080 lb_f (see Figure 14) will exceed the buckling allowable in the cap (assuming it behaves as a pin-pin condition). One must assume the Beechcraft engineers performed this standard stability check at the time of design and, who knows, perhaps came to the conclusion the cap needed to be stabilized, which the shear web would certainly have accomplished.

This idea can be evaluated by performing a buckling analysis check using the classical Euler formulation:

$$F_{crit} = \frac{\pi^2 EI}{(KL)^2}$$

Where; E = Modulus of elasticity = 10.7×10^6 psi (from Reference 5 for 2024-T3)
I = Area moment of inertia = 1.502 in^4 (from the digitized geometry)
L = Beam length (width of spar carry-through) = 46.12 in (from the digitized geometry)
K = Column effective length factor = 1.0 (pin-pin)

Pin-pin boundary conditions:

$$F_{crit} = \frac{\pi^2 (10.7 \times 10^6)(1.502)}{[(1.0)(46.12)]^2} = 74572 \text{ lb}_f$$

This load is less than the load in the member and therefore indicates buckling is a possible failure mode (MS=-0.128). While the author acknowledges the above can be considered speculation, it is considered an important input toward a better understanding of this structure.

Finally this; the author considers the approach recommended by the FAA and ABS, which uses residual strength of the structure as a deciding parameter for continued airworthiness a very sensible approach, and one likely to bear fruit.

REFERENCES

1. *AD 95-04-03*, FAA.
2. *AD 90-08-14*, FAA.
3. *MSB 2269*, Raytheon, August 1989.
4. *MSB 2360*, Raytheon, November 1990.
5. *MIL-HDBK-5J*.
6. *Final Report Submitted by Peter Harradine October 8th 2004*, by Mr. Peter Harradine.
7. *Spar Web Presentation – Part 1*, Article from ABS January 2006. American Bonanza Society.
8. *Report No. ABS36-4004SA*, J.B. Dwerlkotte Associates, Inc.
9. *Analysis and evaluation by Mr. Dick Wilson* (http://mysite.verizon.net/dick.wilson/link2.htm).
10. *2010.0426.Paul Chapman ABS Comments*, by Mr. Paul Chapman (FAA).
11. *2010.0426.Steve Potter ABS Study Comments*, by Mr. Steve Potter (FAA).
12. *July 2009 ABS Spar Web Presentation.pptx*, July 23, 2009. ABS document.
13. *ABS Convention spar web brief.ppt*, Date unknown. ABS document.
14. Type Certificate Data Sheet 3A15.
15. *Letter L115W-09-1174 (from the FAA).pdf*, 01-25-2010, FAA.

APPENDIX A – PROJECT PLAN

RESEARCH PLAN FOR THE AMERICAN BONANZA SOCIETY													
			Software	Engineer 4	Engineer 3	Engineer 2	Engineer 1	Mechanic 3	Mechanic 2	Mechanic 1	Technician 2	Technician 1
				$125	$75	$50	$20	$75	$50	$20	$50	$20
		PHASE I - Preliminary Investigation										
1		Preparation and project organizing		16	4							
2		Investigation of previous work	-	5		20						
3		Acquisition of analysis software	-	5	2	5						
4		Software familiarity or recurrency training	-	4		10	10					
5		Determination of aircraft structural design	-	12	0	40	60	8	0	0	10	10
	a	Detailed geometry	-	6		20	40				10	10
	b	Material identification	-	3		10	10	4				
	c	Fastener identification	-	3		10	10	4				
6		Status report to ABS	-	15	4	40						
		TOTAL		57	10	115	70	8	0	0	10	10
		PHASE II - Research	-									
1		Generation of digital model	Pro/E, CATIA, Solidworks	10	10	100	100					
2		Generation of Finite Element (FE) model	NE NASTRAN	19	0	97	97	0	0	0	0	0
	a	Import geometry		2		5	5					
	b	Create structural elements		5		55	55					
	c	Apply loads		5		20	20					
	d	Solve		2		7	7					
	e	Post-processing		5		10	10					
3		Generation of loads	-	45	30	60	0	0	0	0	0	0
	a	Load analysis per FAR Part 23	-	30	10	30						
	b	Fatigue load analysis	-	15	20	30						
4		Fatigue and Crack-growth analysis	-	4	30	30						
5		Status report to ABS	-	15	4	40						
		TOTAL		93	74	327	197	0	0	0	0	0
		PHASE III - Reporting and Presentation										
1		Report findings and discussions	-	15	10	80						
2		Final report writing	-	30		60						
3		Presentation and final report to the ABS	-	16	16							
		TOTAL		61	26	140	0	0	0	0	0	0

APPENDIX B – RESEARCH PLAN

RESEARCH PLAN					15-Nov	
					Dates	
ID		Task description	Delegatee	Status	Start	End
PHASE I						
I-1		Get material properties	Andrea	50%	6-Sep-2010	15-Oct-2010
I-2		Get fastener types and properties	Andrea	50%	6-Sep-2010	15-Oct-2010
I-3		Digitize the geometry	Lori	100%	6-Sep-2010	26-Sep-2010
I-4		Transfer geometry to CATIA	Lori	100%	6-Sep-2010	26-Sep-2010
I-5		Submit geometry to the FAA for verification	Lori	100%	6-Sep-2010	30-Sep-2010
I-6		Determine air loads per FAR23	Andrea	100%	6-Sep-2010	15-Oct-2010
	a	V-n diagram per FAR23 Sub C	Andrea	100%	6-Sep-2010	15-Oct-2010
	b	Model Bonanza in Surfaces	Ning/Isadora	100%	6-Sep-2010	15-Oct-2010
	c	Retrieve shear and moment diagrams (for 100/70 too)	Ning/Isadora	100%	6-Sep-2010	15-Oct-2010
	d	Determine landing loads per FAR23	Andrea	100%	6-Sep-2010	15-Oct-2010
	e	Evaluate side-loads on nose gear due to ground operations	Andrea	100%	6-Sep-2010	15-Oct-2010
I-7		Get description of airplane from Jane's All the World's AC	Andrea	100%	8-Sep-2010	15-Oct-2010
I-8		Phase I: Status report to ABS	Andrea	50%	15-Oct-2010	15-Nov-2010
PHASE II						
		Generation of Finite Element Model (FEM)				
II-1		Import geometry	Ning/Isadora	25%	15-Nov	15-Dec
II-2		Create structural elements	Ning/Isadora	0%	15-Nov	15-Dec
II-3		Apply loads	Ning/Isadora	0%	15-Nov	15-Dec
II-4		Solve	Ning/Isadora	0%	15-Nov	15-Dec
II-5		Post-processing	Ning/Isadora	0%	15-Nov	15-Dec
		FEM Validation				
II-6		Transport spar carrythrough from Eagleworks to lab	Mike/Zach	100%		
II-7		Instrument spar carrythrough with strain gages	Mike/Zach	0%		
II-8		Collect strain and load information	Mike/Zach	0%		
		Fatigue and Crack-growth analysis				
II-9		Fatigue load analysis	Ning/Isadora	0%	15-Nov	15-Dec
II-10		Fatigue and Crack-growth analysis	Ning/Isadora	0%	15-Nov	15-Dec
II-11		Phase II: Status report to ABS	Andrea(?)	0%	15-Dec	30-Jan
PHASE III						
III-1		Report findings and discussions	Ning/Isadora	0%		
III-2		Final report writing	Ning/Isadora	0%		
III-3		Presentation and final report to the ABS	Ning/Isadora	0%		

APPENDIX C – SELECTED IMAGES FROM CATIA

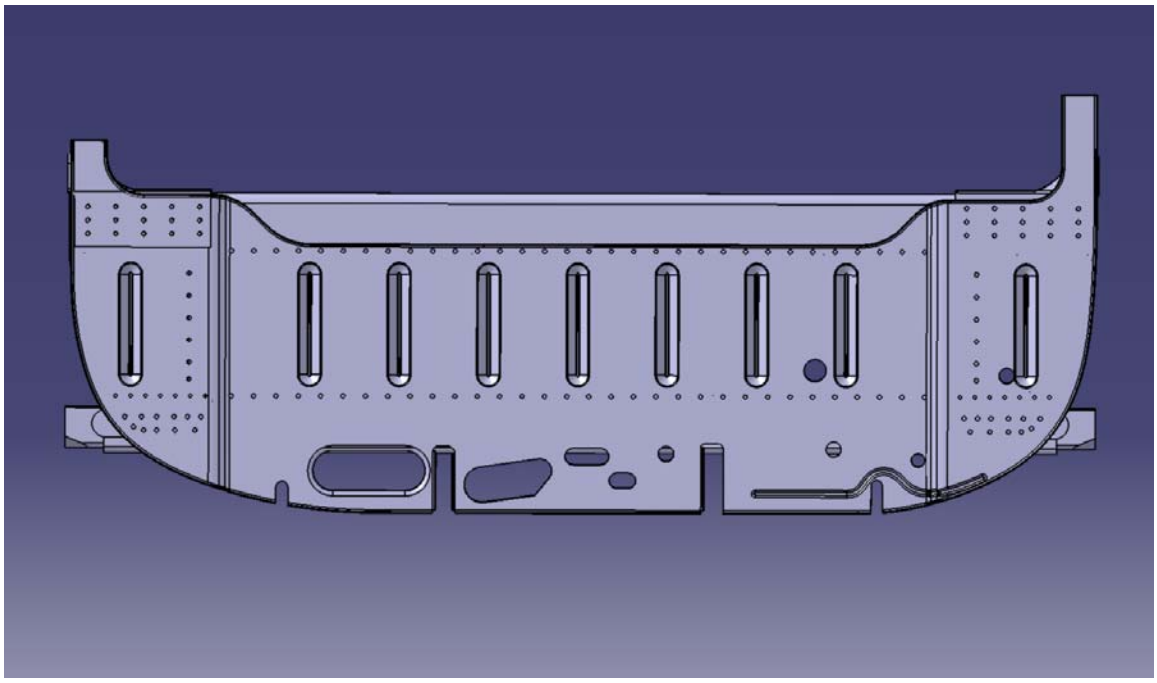

Figure C-1: Spar carry-through assembly front view.

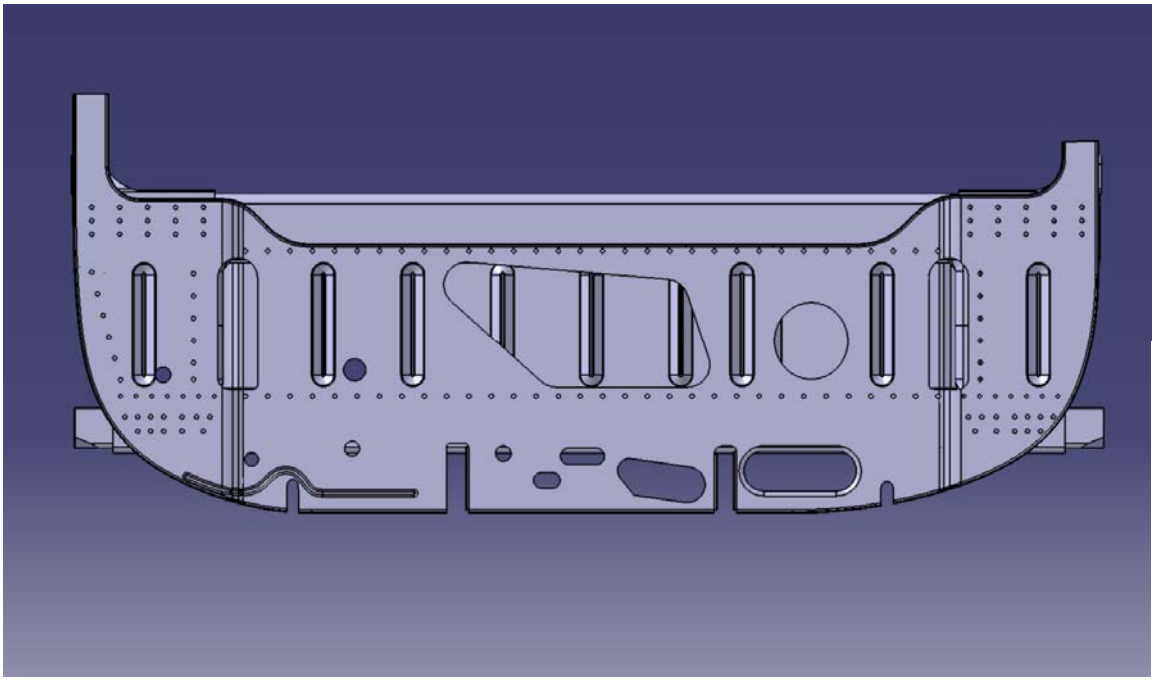

Figure C-2: Spar carry-through assembly rear view. The large opening in the web between the two spars reveals negligible contribution to the reaction of shear by that part.

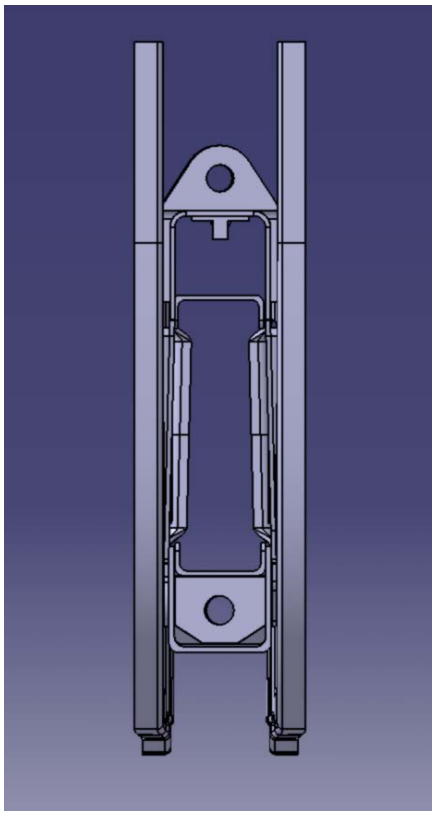

Figure C-3: Spar carry-through assembly side view.

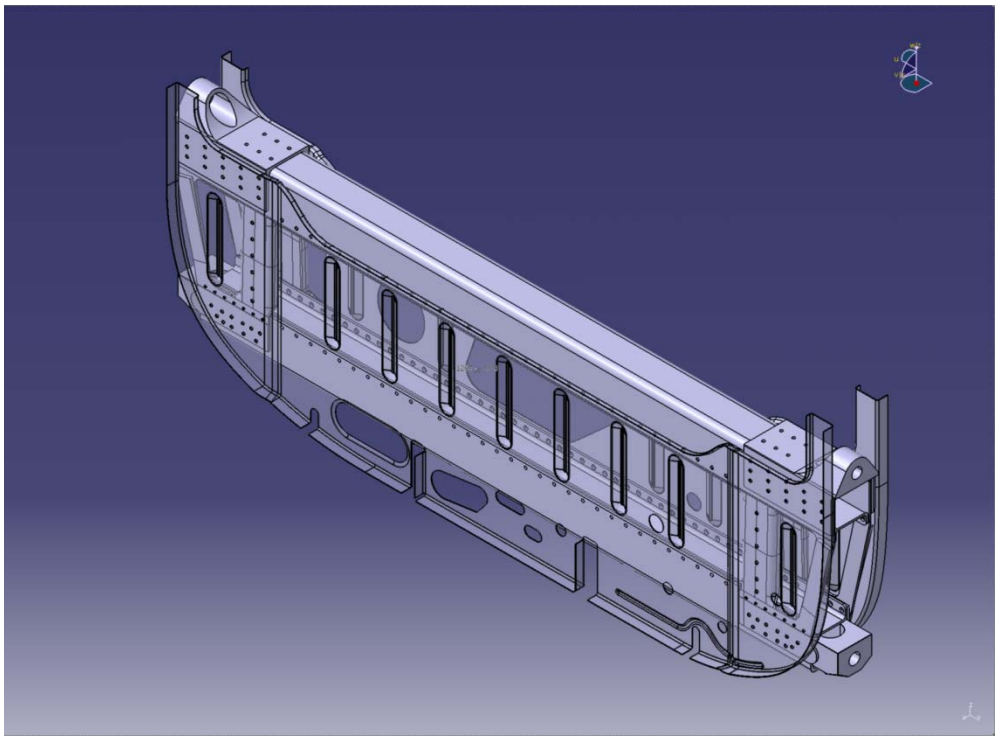

Figure C-4: A phantom view reveals the extent of the spar caps inside the spar carry-through assembly

APPENDIX D – VALIDATION EXAMPLES FOR THE VORTEX-LATTICE SOLVER SURFACES

Validation 9: Comparison to NACA R-1208

V9.1 Introduction

This validation compares **SURFACES** analysis to the swept back wing featured in the NACA report R-1208. In the report a highly swept back, high aspect ratio wing compares three numerical methods to wind tunnel test results. In this validation sample, a similar approach will be taken and the section lift coefficients from **SURFACES** will be compared to the wind tunnel test results. The wing planform is shown in Figure 9-1.

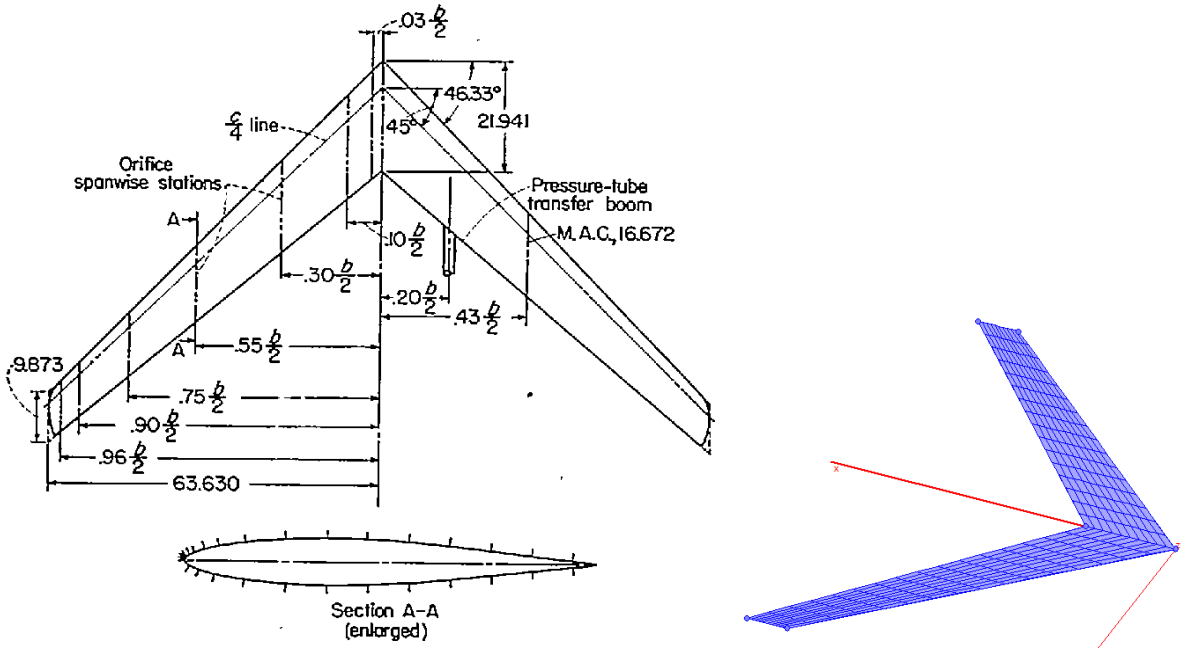

Figure 9-1: The swept-back wing wind tunnel tested per NACA R-1208. Inserted image shows the SURFACES VL model.

Three VL models were generated; one has 16 spanwise panel per wing side, the second one has 32 spanwise panels, and the third has 64 spanwise panels per side. The comparison takes place at 4.7° angle of attack, per the NACA report..

V9.2 Expected Result

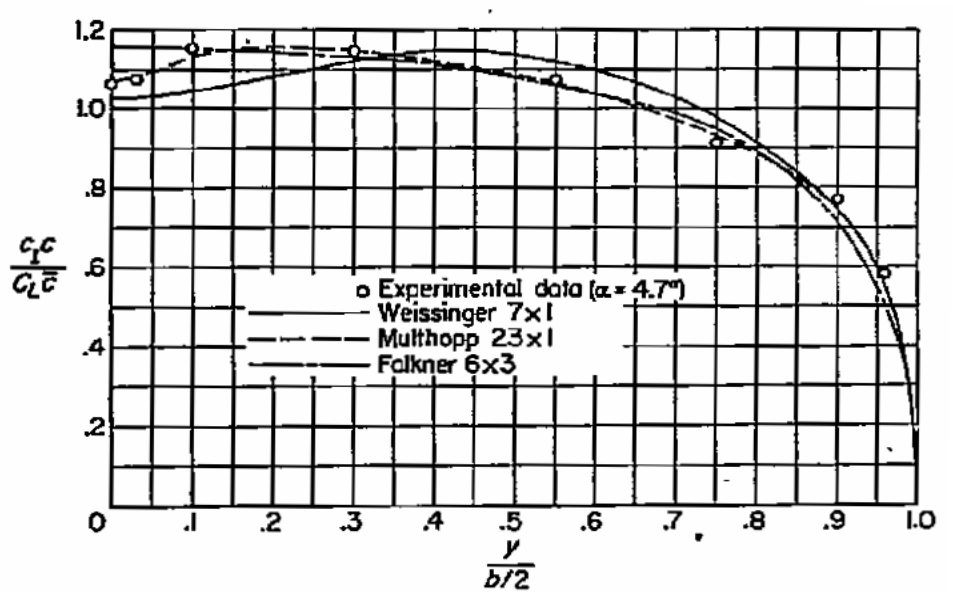

Figure 9-2: Original graph of spanwise loading from NACA R-1208.

V9.3 Results from SURFACES

The comparison of the numerical to the experimental data shows a close agreement, but also that the accuracy improves with number of panels.

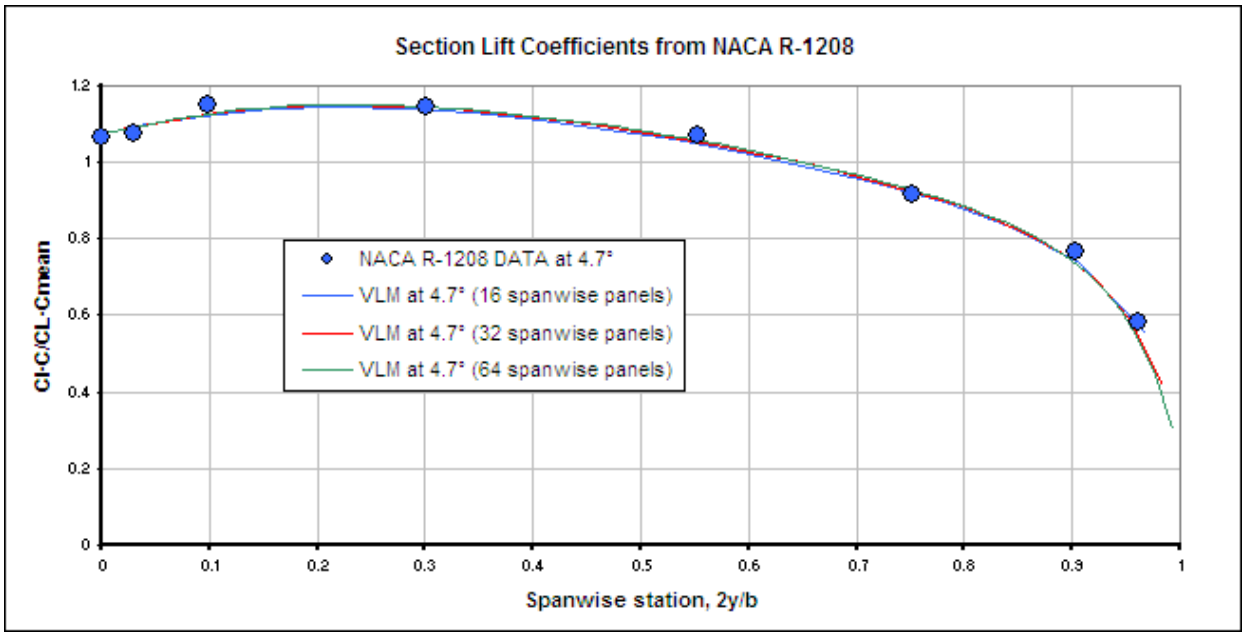

Figure 9-3: Comparing spanwise loading from SURFACES to experimental data from NACA R-1208.

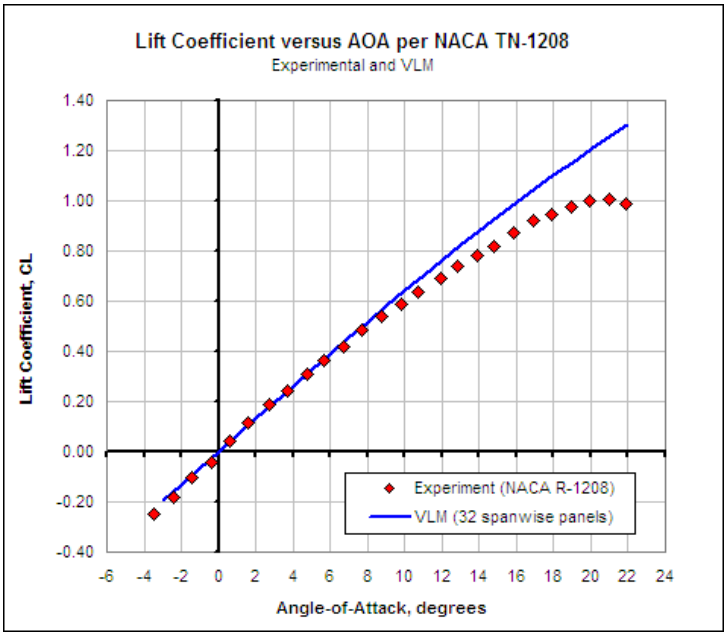

Figure 9-4: Comparing lift curve from SURFACES to experimental data from NACA R-1208.

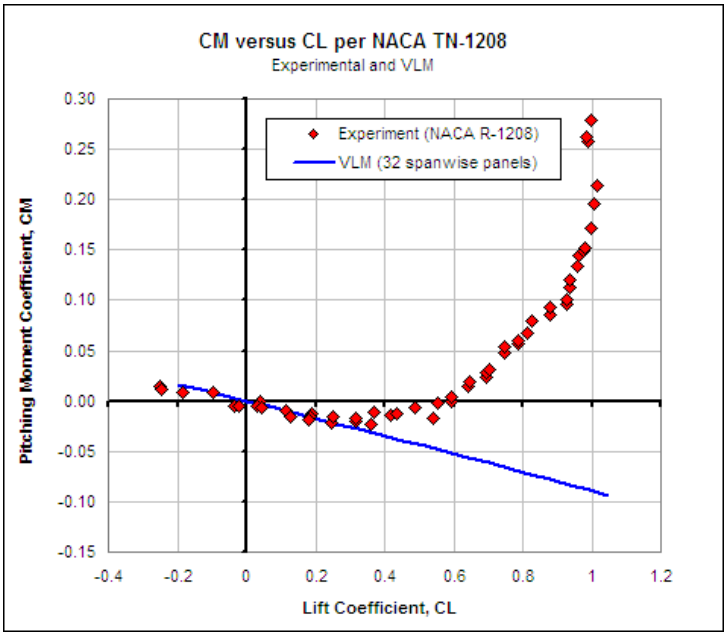

Figure 9-5: Comparing moment curve from SURFACES to experimental data from NACA R-1208. The experimental data shows the well known early tip stall phenomena of swept back wings, caused by spanwise flow near the tips. This is reproduced here to remind the user that all inviscid codes (vortex-lattice, doublet-lattice, panel-codes, etc) do not model this viscous phenomena accurately because the mathematical solution forces the flow to stay attached.

Validation 10: Comparison to NACA TN-1422

V10.1 Introduction

This validation compares **SURFACES** analysis to two of the three tapered and twisted wings featured in the NACA report TN-1422. This report compares several aerodynamic properties of three wings obtained in wind tunnel tests. In this validation sample the section lift coefficients, lift curves, and moment curves for two of these wings (from hereon referred to as WING 2 and WING 3) from **SURFACES** will be compared to the wind tunnel test results. The general planform shape is shown in Figure 10-1, and is reproduced from the original document.

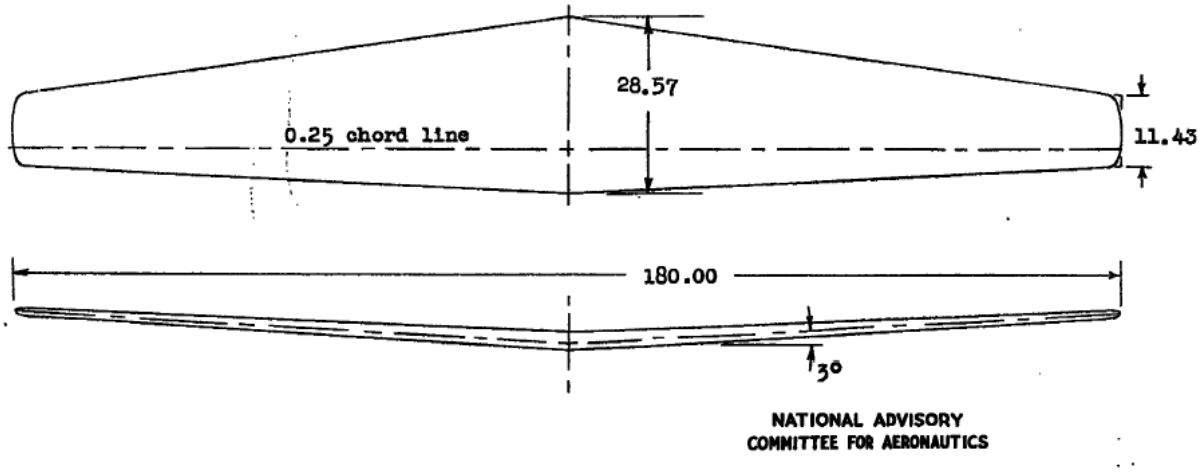

Figure 1.- General dimensions of 10-percent-thick wings tested in Langley 19-foot pressure tunnel. Aspect ratio, 9; ratio of root chord to tip chord, 2.5. (All dimensions are in inches.)

Figure 10-1: The general shape of the wind tunnel model tested per NACA TN-1422.

V10.2 Results from SURFACES

The comparison of the numerical to the experimental data shows a close agreement.

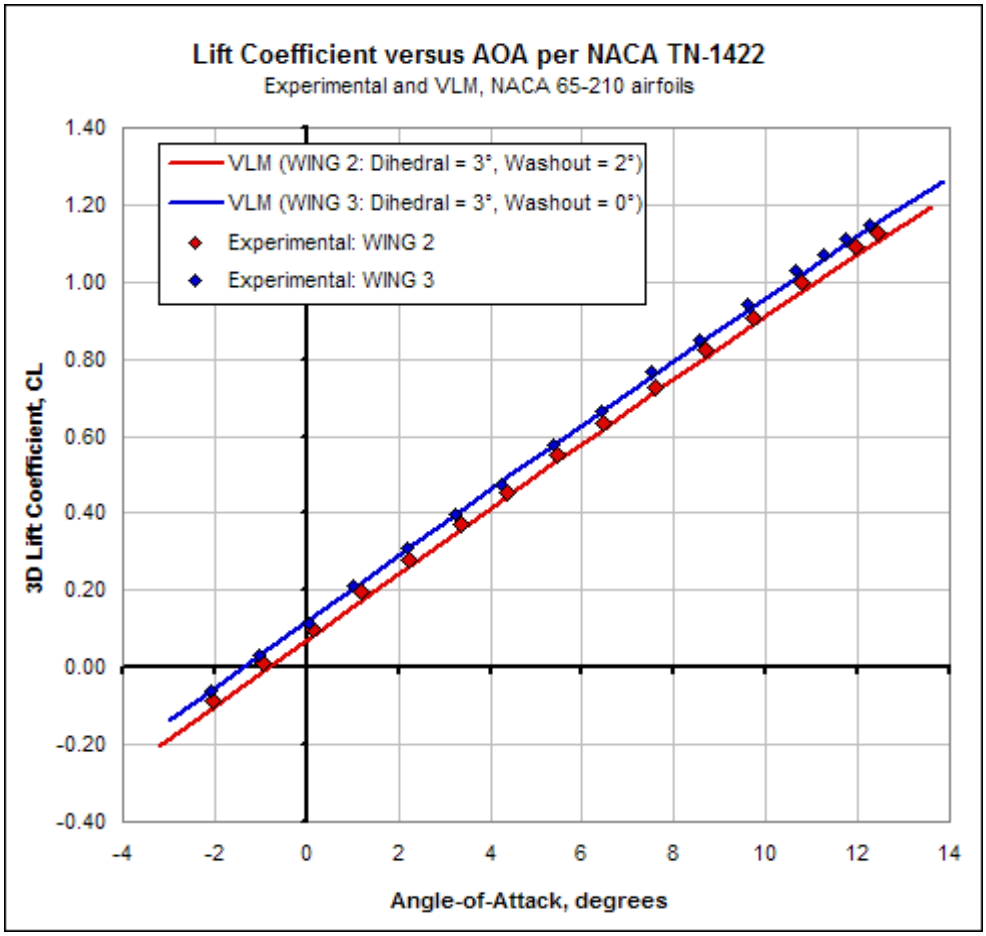

Figure 10-2: Match for the lift curve for the twisted and untwisted wings.

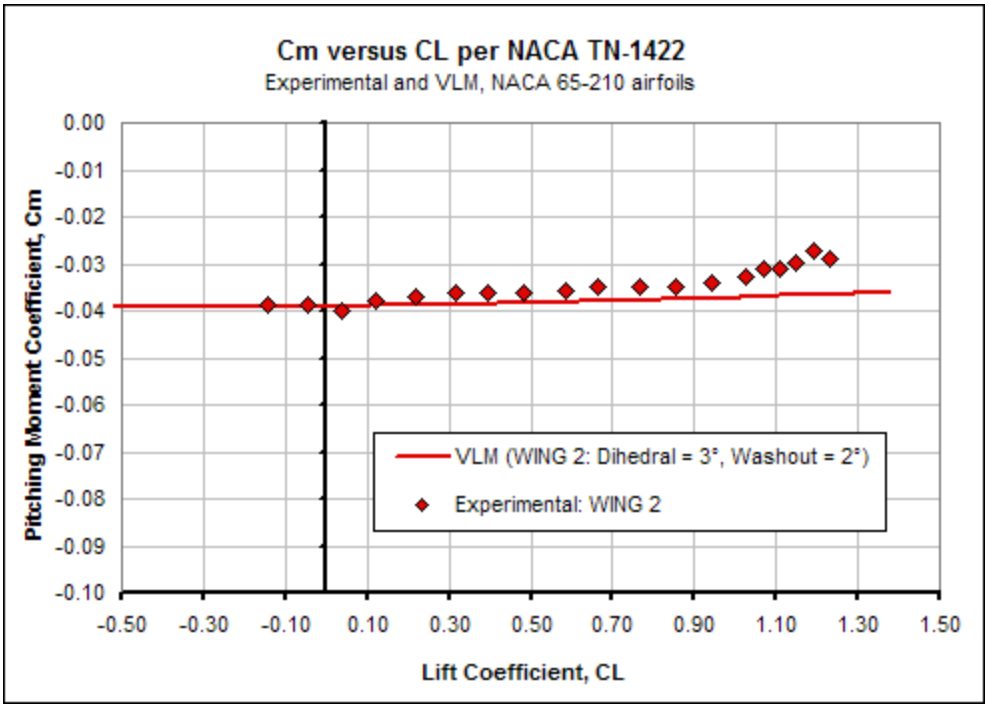

Figure 10-3: Match for the pitching moment for the twisted wing. Note the deviation at higher values of the lift coefficient, which is caused by viscous effects.

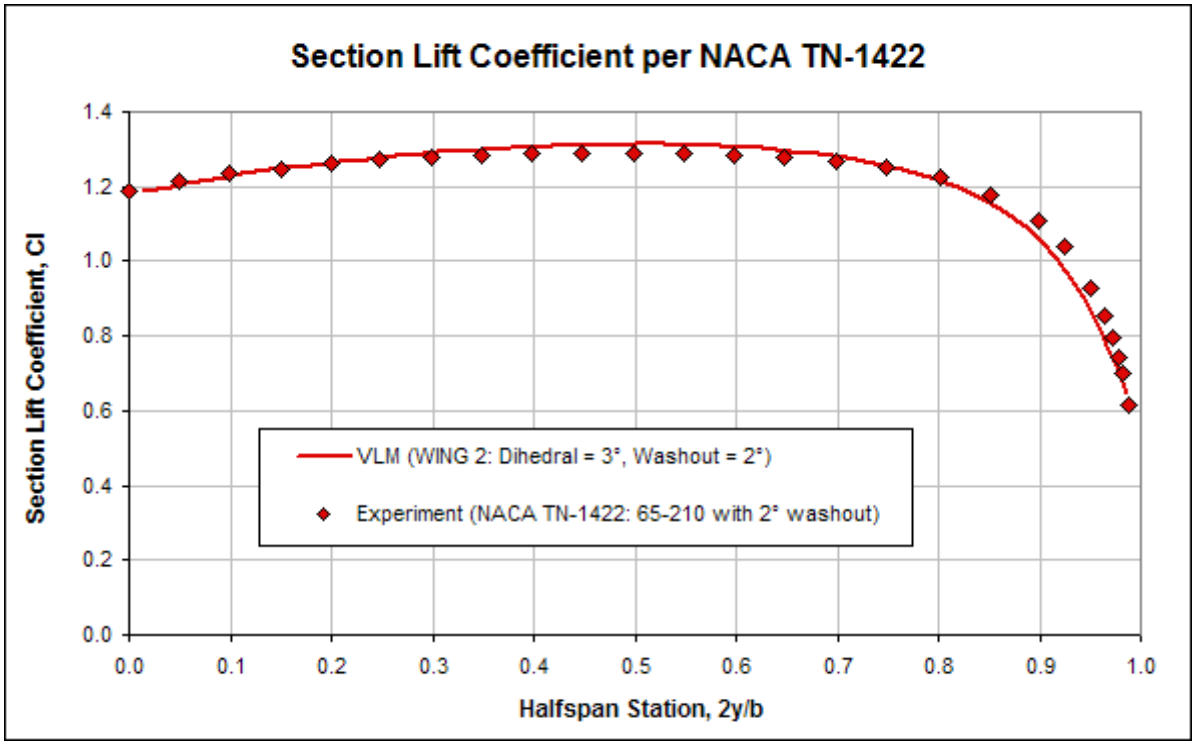

Figure 10-4: Lift distribution at stall for the twisted wing.

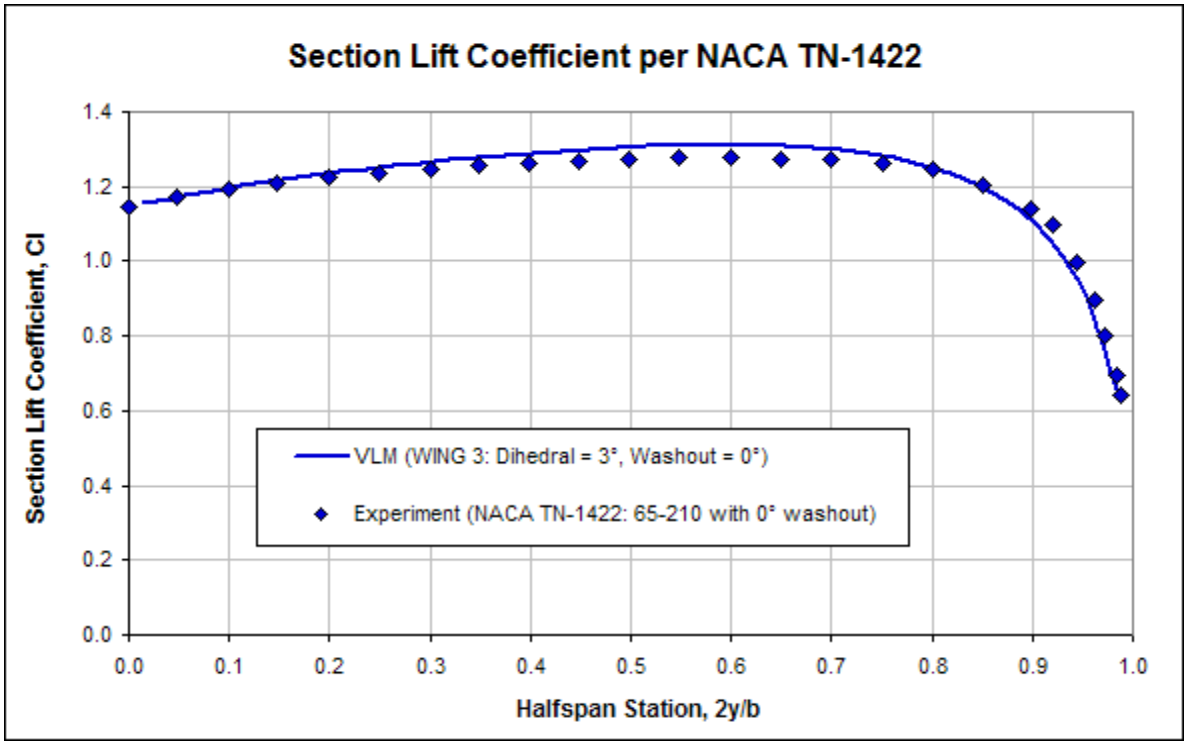

Figure 10-5: Lift distribution at stall for the untwisted wing.

APPENDIX E – POSITION LETTER FROM FAA ACO TO ABS

U.S. Department
of Transportation
**Federal Aviation
Administration**

Small Airplane Directorate
Wichita Aircraft Certification Office
1801 Airport Road, Room 100
Wichita, Kansas 67209

January 25, 2010

L115W-09-1174

Mr. Thomas P. Turner
Manager of Technical Services
American Bonanza Society (ABS)
Headquarters
P. O. Box 12888
Wichita, Ks 67277

Subject: FAA Review of ABS Engineering Study, Hawker Beechcraft Corporation (HBC) Models Bonanza and Baron Wing Center Section

Reference: (1) ABS072007-005, Rev. IR, July 20, 2009, Lower Forward Spar Web Investigation Beechcraft V35B/V36 Bonanza
(2) ABS072007-005, Appendix D, Rev. IR, September 9, 2009, Damage Tolerance Analysis Beechcraft V35B/A36 Bonanza

Dear Mr. Turner:

The Wichita Aircraft Certification Office (ACO) has reviewed and evaluated the referenced reports. Your work and understanding of this complex problem is highly appreciated and recognized; however to fully address safety this office still feels more effort is required. We make the following comments and recommendation for further efforts.

Item (1) Validation of the Finite Element Model is valuable in order to increase confidence in the analysis. Typically some independent confirmation of the model; such as flight test, ground test, elementary beam theory hand-calculations are accomplished. We did find two hand analysis correlations on pages B22 and B44. The model does appear to predict logical results, but the ACO engineers would like to have further discussion with your consultants on some specific details.

Item (2) The report presented rational loads analysis for the loading conditions which are most probable contributors to the web cracking around the Huck bolt collars. After review of the Normal Operating Procedures in the Pilot Operating Handbook, it appears that a condition more conservative than those presented would be Take-Off Full Power (set brakes, apply full power, release brakes). It would be prudent to add this condition to the analysis.

Item (3) In order to ensure safety any damage tolerance analysis needs to check for critical crack scenarios using residual strength methods. The report presented one static scenario as a worst case analysis. The condition may or may not be worst case. In order to be confident

of the residual strength capability, ACO engineers propose additional crack types & scenarios as listed in ADs 95-04-03 and 90-08-14.

1) One 2.25 inch crack on either side of the front spar.

2) More than one 2.25 inch crack on either side of the front spar.

3) One 4.00 inch crack on either side of the front spar.

4) More than one 4.00 inch crack on either side of the front spar

5) One 1.00 inch crack on either side of the front spar.

6) More than 1.00 inch crack on either side of the front spar.

7) A crack passing through two fasteners on one side of the front spar.

8) More than one crack passing through two fasteners on one side of the front spar.

9) A crack in the Huck Bolt area and a crack in the bend radius.

10) An additional crack scenario not defined in the AD's which should be investigated is multi-site cracking in one web at all Huck bolts disabling the shear connection of that web.

In addition to the cases above further investigation of the scenario presented in §4.1.2 Post Crack Structural Capability should be done to ensure no stability concerns exist for any of the failure conditions.

In-service cracking can be affected by multiple factors. Our goal is to examine the structure to ensure we encompass the problem and understand as much about the residual strength scenarios as possible. Evaluation of these conditions will help satisfy concerns of multiple cracks existing and the possibly of linking up. The ACO engineers would be glad to work with your consultant engineers in order to capture the array of cracking scenarios.

After your review of this letter, we may need additional discussions or meetings. Again, your work, effort and understanding in these continued airworthiness matters are greatly appreciated.

Sincerely,

Paul (Vu) Nguyen
Continued Operational Safety (COS) Program Manager
Wichita Aircraft Certification Office

APPENDIX F – RESEARCH TEAM STATUS REPORT

Status Report

FATIGUE CRACK INVESTIGATION IN THE WING CARRY-THRU STRUCTURE OF THE BEECHCRAFT BONANZA

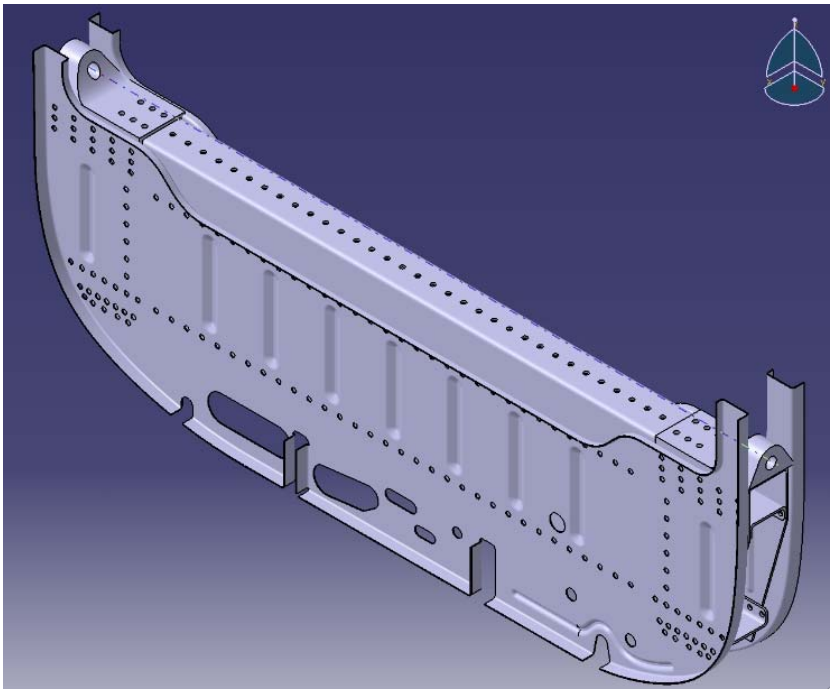

Research Team

Andrea E. Palacios, Isadora P. Thisted, Ning Leung, Michael D. Scheppa, Christopher Foti, Zachary D. Sager

Supervisors

Snorri Gudmundsson and Eric v. K. Hill

Aerospace Engineering Department
Embry Riddle Aeronautical University, Daytona Beach, FL 32114-3900

November 15, 2010

1. Project Overview:

A number of Beechcraft Bonanza aircraft have been plagued with cracks on their front spar carry-thru structure. The cracks primarily form on the front shear panel of the structure in the general vicinity of the so-called huck bolts. A front spar carry-thru structure from a Beechcraft Bonanza, affected by a fatigue crack, was obtained for analysis and testing. Examination of the structure revealed a crack that was located between the huck bolts on the lower left side of the front shear panel. The first step in this project was to digitize the structure into a three dimensional CATIA model. After a detailed analysis, the maximum loads the structure would experience were identified. Utilizing the calculated load values, the stresses in the area surrounding the crack can be approximated using Finite Element Analysis (FEA). A fatigue test will then be performed on the structure and the resulting data will be used to validate the FEA model. During the fatigue test, acoustic emission transducers will be used to collect data that will help determine the critical crack length. Currently, FAA airworthiness directives state that fatigue cracks must be fixed immediately.

2. Detailed Report

2.1 Geometry Digitization and CATIA

Pictures of the front and side views of the part were taken using a digital camera and a tripod. These images were loaded into CATIA and used as a template for modeling the structure. Additional Measurements were taken using calipers and other measuring instruments. A screen shot of the model can be found below in Figure 1.

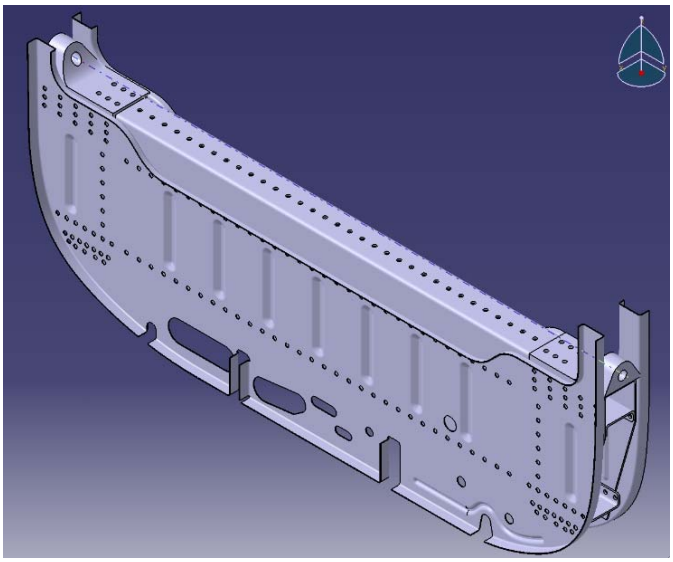

Figure 1: Snapshot of the digitized structure in CATIA.

2.2 Air Loads

The ultimate load factors were obtained from the FARs specifications for aerobatic aircraft. The following parameters were calculated: cruise lift coefficient, maximum lift coefficient with and maximum lift coefficient without flaps. $C_{L\alpha}$ was approximated to be 4.78. Four different scenarios were analyzed for each of the aerobatic and the utility variants of the aircraft: at sea level and cruise altitude (6000 ft) with and without flaps. The plots shown below illustrate the flight envelope at sea level for both the aerobatic and utility aircraft based on the calculated values.

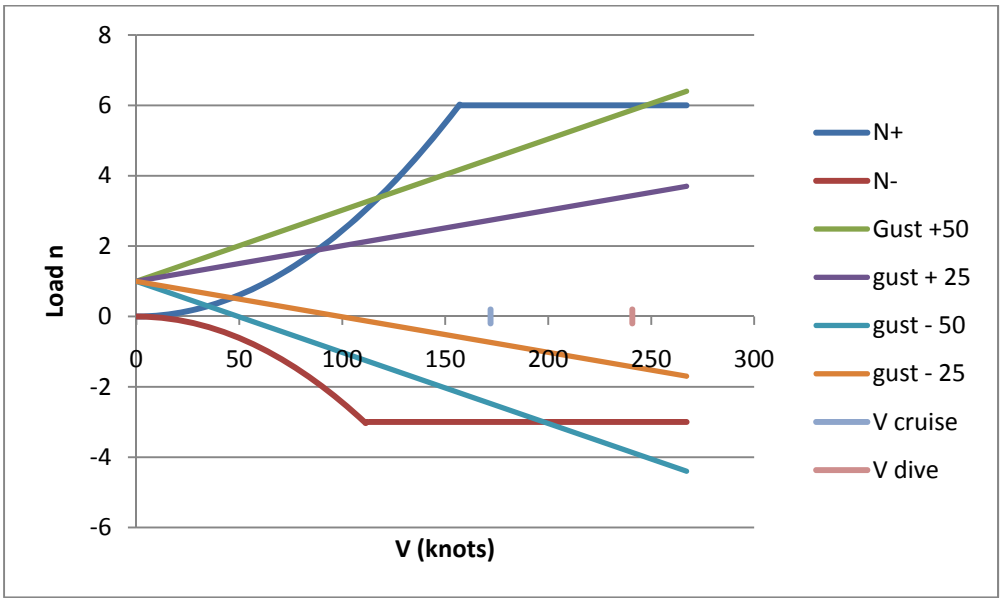

Figure 2: Sea level flight envelope for aerobatic variant

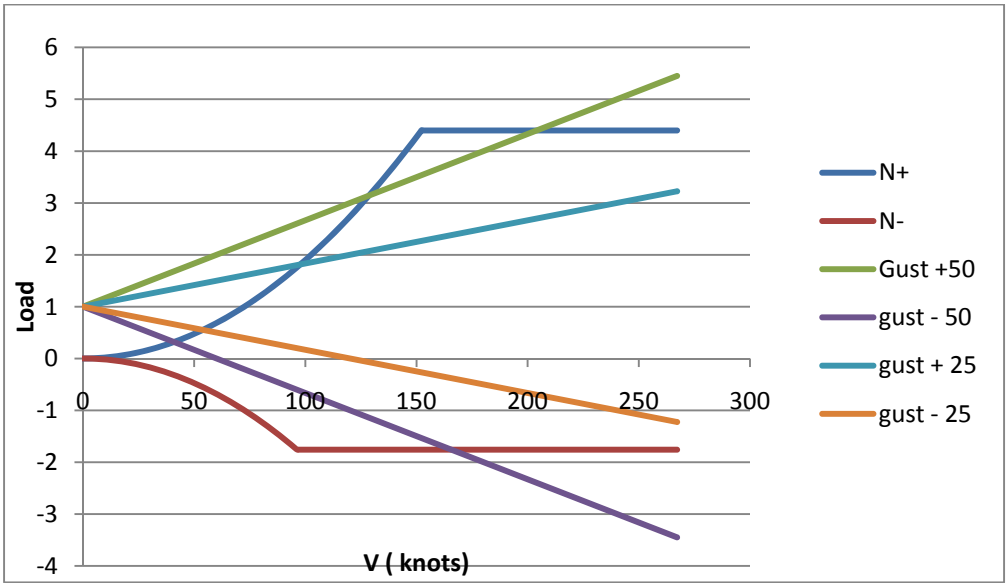

Figure 3: Sea level flight envelope for utility variant

The load factor taken from the FAR section 23.337(A.01) for acrobatic aircraft was 6G's in the positive direction and -3G's in the negative direction. For utility aircraft the positive load is 4.4G's and the negative is -1.76G's. The aircraft dimensions were taken from a scaled drawing of a Beechcraft Bonanza A36 (A.02). The values for these dimensions will be updated later with information from the aircraft's maintenance manual and blueprints.

2.3 Landing Gear Loads – Ground Loads – Side Loads

The limit load factors for the nose gear were found for 3 critical cases; vertical and forward load acting together, vertical and drag load acting together and vertical and side load acting together. The results on the nose landing gear are summarized in the tables below.

Description – Static Loads	Utility	Aerobatic	
Max Static Load	3471	2700	lb_f
Max Static Load Nose	236	183	lb_f
Min Static Load Nose	129	100	lb_f
Dynamic Breaking Load Nose	503	391	lb_f

Description – Limit Loads	Utility	Aerobatic	
Vertical Component	530	413	lb_f
Drag Component	424	330	lb_f
Forward Component	212	165	lb_f
Side Component	371	289	lb_f

The drag loads, side loads and forward loads are all a function of the vertical component of the load, which is specified in the FAR Section 23.499(A.03). Therefore, from the above results, it is clear when both static and dynamic loads are present; the worst case scenario for all calculated loads comes from the drag components.

The main gear loads depend on the landing contact velocity which was found to be 9.29 ft/s for utility and 8.72 ft/s for the aerobatic configuration. This would allow calculations on loads and forces of each tire from the main gear. The calculation of the main landing gear loads are based on the FARs 23.473(A.04) and 23.485 (A.05); results acquired from FAR's parts 23.473 and 23.485 are shown below.

Description – Limit Loads	Utility	Aerobatic	
Inertia Load Factor	3.0	3.0	
Force Applied On Each Wheel	4200	5400	lb_f
Side Force	2332	2999	lb_f
Inboard Force	1400	1800	lb_f
Outboard Force	924	1188	lb_f
Drag Reaction	3360	4320	lb_f

The results above show that, similarly to the nose landing gear, drag is the worst case scenario for landing loads.

The Civil Air Regulation (CAR) was the regulation in effect at the time the airplane was designed. For the purpose of understanding the criteria under which the aircraft was designed, the regulations from the CAR were compared to current regulations from the FAR. A major difference is stated in section 23.499 part (d) and (e) of the FARs. Section 23.499 part (d) states:

> "For airplanes with a steerable nose wheel that is controlled by hydraulic or other power, at design take- off weight with the nose wheel in any steerable position, the application of 1.33 times the full steering torque combined with a vertical reaction equal to 1.33 times the maximum static reaction on the nose gear must be assumed. However, if a torque limiting device is installed, the steering torque can be reduced

to the maximum value allowed by that device."

And Section 23.499 part (e) states:

> "For airplanes with a steerable nose wheel that has a direct mechanical connection to the rudder pedals, the mechanism must be designed to withstand the steering torque for the maximum pilot forces specified in § 23.397(b)."

2.4 Shear and Moment Diagram

The calculations of the shear and moment reactions on the wings of the Beechcraft Bonanza F33C were calculated using Surfaces, a computer program that utilizes the Vortex Lattice Method (VLM) in its computations. The aircraft was modeled in Surfaces by utilizing dimensions acquired from three orthographic views (A.02). The program works by dividing an aircraft surface into a user specified number of panels, calculating all forces acting on each panel and subsequently summing those forces. Surfaces allows the user to input many parameters such as weight, airspeed, wing geometry and load factors which can be used to evaluate solutions in a number of different scenarios. The air load analyses for both the utility and the aerobatic configurations of the Bonanza were performed.

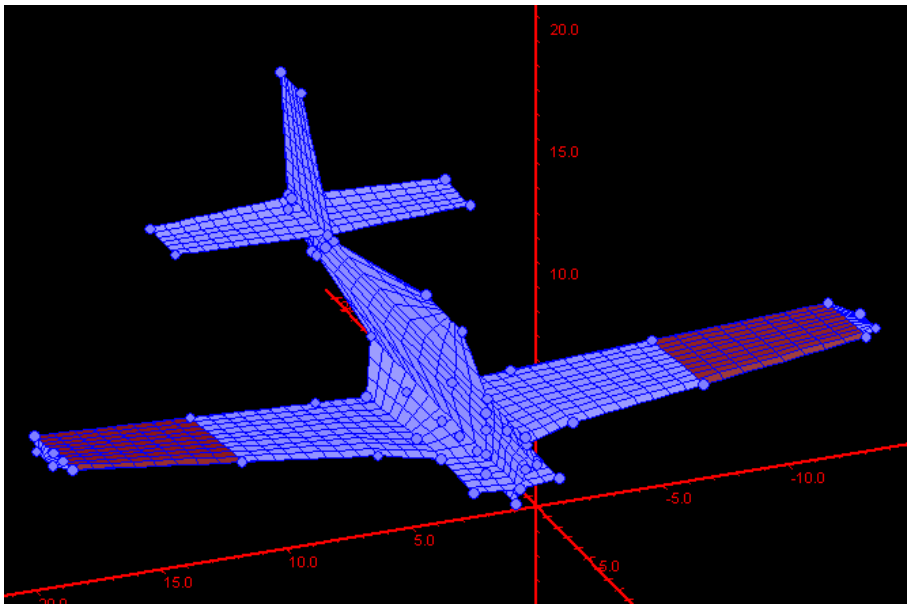

Figure 4: Beechcraft Bonanza F33C Model in Surfaces.

In accordance with FAR23 (A.01), the maximum load factors for the utility configuration is 4.4G's, while the aerobatic configuration is rated to withstand 6.0G's. The program trimmed the model to level flight at both the maneuvering and max diving speeds for both configurations of the aircraft. The maneuvering speed information was determined from the aircraft's V-n diagram while the maximum diving speed was obtained from the FAA Type Certification Documentation (A.07).

The program outputs a spreadsheet that contains all the force values calculated for each panel. From these results, we were able to compute the moment acting at each location of the wing. An outline of the procedure used to calculate the moments can be found in appendix A.08. From our

calculations the maximum moment generated by the air loads at the wing-spar attachment point was of 50,260 lb·ft. This moment was obtained from the scenario of an aerobatic aircraft cruising at the maneuvering airspeed with a load factor of 6G's.

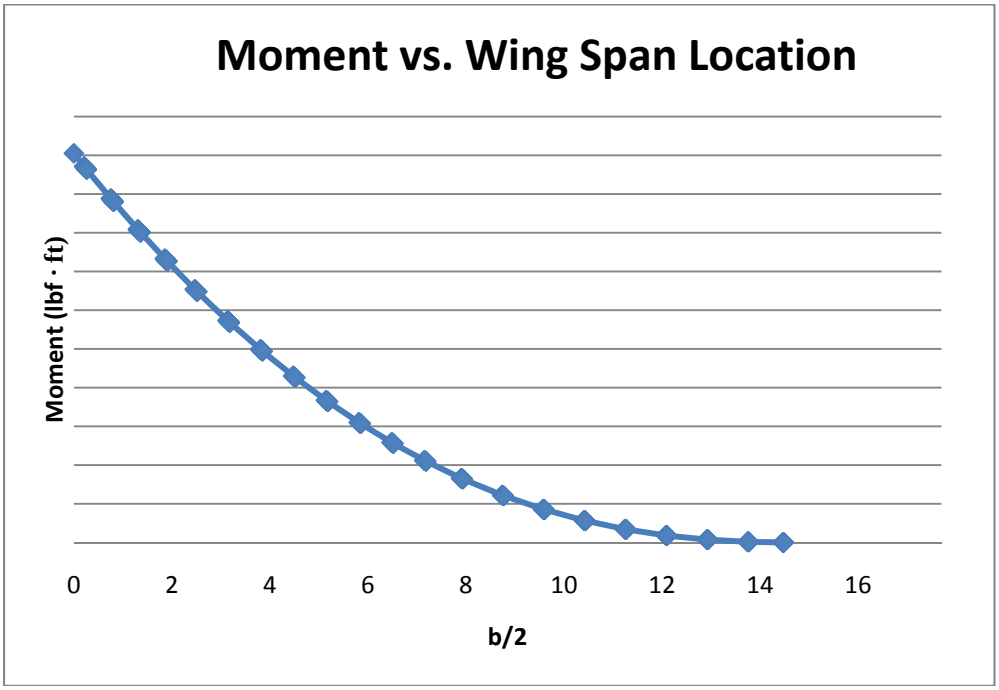

Figure 5: Bending Moment diagram for aerobatic variation at 6G's and 155 Knots CAS

EMBRY-RIDDLE AERONAUTICAL UNIVERSITY

Appendix

A.01 – FAR23.337 Limit maneuvering load factors for acrobatic category airplanes.

(ii) Mach 0.05 for normal, utility, and acrobatic category airplanes (at altitudes where M_D is established); or

(iii) Mach 0.07 for commuter category airplanes (at altitudes where M_D is established) unless a rational analysis, including the effects of automatic systems, is used to determine a lower margin. If a rational analysis is used, the minimum speed margin must be enough to provide for atmospheric variations (such as horizontal gusts), and the penetration of jet streams or cold fronts), instrument errors, airframe production variations, and must not be less than Mach 0.05.

(c) *Design maneuvering speed* V_A. For V_A, the following applies:

(1) V_A may not be less than $V_S\sqrt{n}$ where—

(i) V_S is a computed stalling speed with flaps retracted at the design weight, normally based on the maximum airplane normal force coefficients, C_{NA}; and

(ii) n is the limit maneuvering load factor used in design

(2) The value of V_A need not exceed the value of V_C used in design.

(d) *Design speed for maximum gust intensity,* V_B. For V_B, the following apply:

(1) V_B may not be less than the speed determined by the intersection of the line representing the maximum positive lift, C_{NMAX}, and the line representing the rough air gust velocity on the gust V-n diagram, or $V_{S1}\sqrt{n_g}$, whichever is less, where:

(i) n_g the positive airplane gust load factor due to gust, at speed V_C (in accordance with § 23.341), and at the particular weight under consideration; and

(ii) V_{S1} is the stalling speed with the flaps retracted at the particular weight under consideration.

(2) V_B need not be greater than V_C.

[Doc. No. 4080, 29 FR 17955, Dec. 18, 1964, as amended by Amdt. 23-7, 34 FR 13088, Aug. 13, 1969; Amdt. 23-16, 40 FR 2577, Jan. 14, 1975; Amdt. 23-34, 52 FR 1829, Jan. 15, 1987; Amdt. 23-24, 52 FR 34745, Sept. 14, 1987; Amdt. 23-48, 61 FR 5143, Feb. 9, 1996]

§ 23.337 Limit maneuvering load factors.

(a) The positive limit maneuvering load factor n may not be less than—

(1) 2.1+(24,000÷(W+10,000)) for normal and commuter category airplanes, where W=design maximum takeoff weight, except that n need not be more than 3.8;

(2) 4.4 for utility category airplanes; or

(3) 6.0 for acrobatic category airplanes.

(b) The negative limit maneuvering load factor may not be less than—

(1) 0.4 times the positive load factor for the normal utility and commuter categories; or

(2) 0.5 times the positive load factor for the acrobatic category.

(c) Maneuvering load factors lower than those specified in this section may be used if the airplane has design features that make it impossible to exceed these values in flight.

[Doc. No. 4080, 29 FR 17955, Dec. 18, 1964, as amended by Amdt. 23-7, 34 FR 13088, Aug. 13, 1969; Amdt. 23-34, 52 FR 1829, Jan. 15, 1987; Amdt. 23-48, 61 FR 5144, Feb. 9, 1996]

§ 23.341 Gust loads factors.

(a) Each airplane must be designed to withstand loads on each lifting surface resulting from gusts specified in § 23.333(c).

(b) The gust load for a canard or tandem wing configuration must be computed using a rational analysis, or may be computed in accordance with paragraph (c) of this section, provided that the resulting net loads are shown to be conservative with respect to the gust criteria of § 23.333(c).

(c) In the absence of a more rational analysis, the gust load factors must be computed as follows—

$$n = 1 + \frac{K_g U_{de} V a}{498\,(W/S)}$$

Where—

K_g=0.88μ_g/5.3+μ_g=gust alleviation factor;

μ_g=2(W/S)/ρ Cag=airplane mass ratio;

U_{de}=Derived gust velocities referred to in § 23.333(c) (f.p.s.);

ρ=Density of air (slugs/cu.ft.);

W/S=Wing loading (p.s.f.) due to the applicable weight of the airplane in the particular load case.

W/S=Wing loading (p.s.f.);

C=Mean geometric chord (ft.);

g=Acceleration due to gravity (ft./sec.²)

V=Airplane equivalent speed (knots); and

a=Slope of the airplane normal force coefficient curve C_{NA} per radian if the gust loads are applied to the wings and horizontal tail

A.02 – Bonanza A36 scaled model.

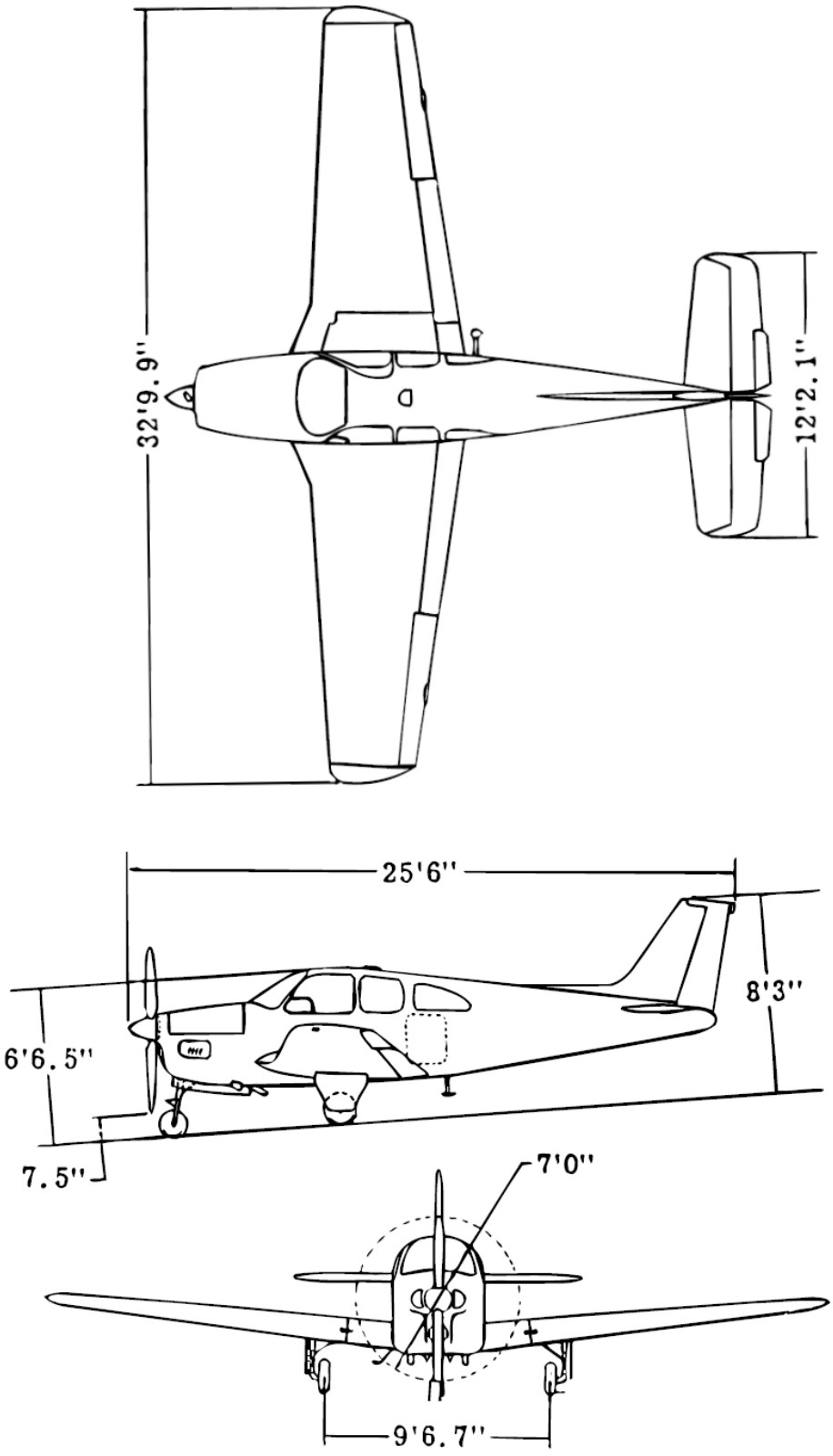

A.03 - Vertical Components and supplementary conditions for nose wheel.

and the drag loads may be assumed to be zero.

[Doc. No. 4080, 29 FR 17955, Dec. 18, 1964, as amended by Amdt. 23-45, 58 FR 42160, Aug. 6, 1993]

§23.493 Braked roll conditions.

Under braked roll conditions, with the shock absorbers and tires in their static positions, the following apply:

(a) The limit vertical load factor must be 1.33.

(b) The attitudes and ground contacts must be those described in §23.479 for level landings.

(c) A drag reaction equal to the vertical reaction at the wheel multiplied by a coefficient of friction of 0.8 must be applied at the ground contact point of each wheel with brakes, except that the drag reaction need not exceed the maximum value based on limiting brake torque.

§23.497 Supplementary conditions for tail wheels.

In determining the ground loads on the tail wheel and affected supporting structures, the following apply:

(a) For the obstruction load, the limit ground reaction obtained in the tail down landing condition is assumed to act up and aft through the axle at 45 degrees. The shock absorber and tire may be assumed to be in their static positions.

(b) For the side load, a limit vertical ground reaction equal to the static load on the tail wheel, in combination with a side component of equal magnitude, is assumed. In addition—

(1) If a swivel is used, the tail wheel is assumed to be swiveled 90 degrees to the airplane longitudinal axis with the resultant ground load passing through the axle;

(2) If a lock, steering device, or shimmy damper is used, the tail wheel is also assumed to be in the trailing position with the side load acting at the ground contact point; and

(3) The shock absorber and tire are assumed to be in their static positions.

(c) If a tail wheel, bumper, or an energy absorption device is provided to show compliance with §23.925(b), the following apply:

(1) Suitable design loads must be established for the tail wheel, bumper, or energy absorption device; and

(2) The supporting structure of the tail wheel, bumper, or energy absorption device must be designed to withstand the loads established in paragraph (c)(1) of this section.

[Doc. No. 4080, 29 FR 17955, Dec. 18, 1964, as amended by Amdt. 23-48, 61 FR 5147, Feb. 9, 1996]

§23.499 Supplementary conditions for nose wheels.

In determining the ground loads on nose wheels and affected supporting structures, and assuming that the shock absorbers and tires are in their static positions, the following conditions must be met:

(a) For aft loads, the limit force components at the axle must be—

(1) A vertical component of 2.25 times the static load on the wheel; and

(2) A drag component of 0.8 times the vertical load.

(b) For forward loads, the limit force components at the axle must be—

(1) A vertical component of 2.25 times the static load on the wheel; and

(2) A forward component of 0.4 times the vertical load.

(c) For side loads, the limit force components at ground contact must be—

(1) A vertical component of 2.25 times the static load on the wheel; and

(2) A side component of 0.7 times the vertical load.

(d) For airplanes with a steerable nose wheel that is controlled by hydraulic or other power, at design takeoff weight with the nose wheel in any steerable position, the application of 1.33 times the full steering torque combined with a vertical reaction equal to 1.33 times the maximum static reaction on the nose gear must be assumed. However, if a torque limiting device is installed, the steering torque can be reduced to the maximum value allowed by that device.

(e) For airplanes with a steerable nose wheel that has a direct mechanical connection to the rudder pedals, the mechanism must be designed to withstand the steering torque for the

A.04 - Ground load conditions and assumptions.

(2) By the following deflections (except as limited by pilot effort), during unsymmetrical flight conditions:

(i) Sudden maximum displacement of the aileron control at V_A. Suitable allowance may be made for control system deflections.

(ii) Sufficient deflection at V_C, where V_C is more than V_A, to produce a rate of roll not less than obtained in paragraph (a)(2)(i) of this section.

(iii) Sufficient deflection at V_D to produce a rate of roll not less than one-third of that obtained in paragraph (a)(2)(i) of this section.

(b) [Reserved]

[Doc. No. 4080, 29 FR 17955, Dec. 18, 1964, as amended by Amdt. 23-7, 34 FR 13090, Aug. 13, 1969; Amdt. 23-42, 56 FR 353, Jan. 3, 1991]

§23.459 Special devices.

The loading for special devices using aerodynamic surfaces (such as slots and spoilers) must be determined from test data.

GROUND LOADS

§23.471 General.

The limit ground loads specified in this subpart are considered to be external loads and inertia forces that act upon an airplane structure. In each specified ground load condition, the external reactions must be placed in equilibrium with the linear and angular inertia forces in a rational or conservative manner.

§23.473 Ground load conditions and assumptions.

(a) The ground load requirements of this subpart must be complied with at the design maximum weight except that §§23.479, 23.481, and 23.483 may be complied with at a design landing weight (the highest weight for landing conditions at the maximum descent velocity) allowed under paragraphs (b) and (c) of this section.

(b) The design landing weight may be as low as—

(1) 95 percent of the maximum weight if the minimum fuel capacity is enough for at least one-half hour of operation at maximum continuous power plus a capacity equal to a fuel weight which is the difference between the design maximum weight and the design landing weight; or

(2) The design maximum weight less the weight of 25 percent of the total fuel capacity.

(c) The design landing weight of a multiengine airplane may be less than that allowed under paragraph (b) of this section if—

(1) The airplane meets the one-engine-inoperative climb requirements of §23.67(b)(1) or (c); and

(2) Compliance is shown with the fuel jettisoning system requirements of §23.1001.

(d) The selected limit vertical inertia load factor at the center of gravity of the airplane for the ground load conditions prescribed in this subpart may not be less than that which would be obtained when landing with a descent velocity (V), in feet per second, equal to 4.4 $(W/S)^{1/4}$, except that this velocity need not be more than 10 feet per second and may not be less than seven feet per second.

(e) Wing lift not exceeding two-thirds of the weight of the airplane may be assumed to exist throughout the landing impact and to act through the center of gravity. The ground reaction load factor may be equal to the inertia load factor minus the ratio of the above assumed wing lift to the airplane weight.

(f) If energy absorption tests are made to determine the limit load factor corresponding to the required limit descent velocities, these tests must be made under §23.723(a).

(g) No inertia load factor used for design purposes may be less than 2.67, nor may the limit ground reaction load factor be less than 2.0 at design maximum weight, unless these lower values will not be exceeded in taxiing at speeds up to takeoff speed over terrain as rough as that expected in service.

[Doc. No. 4080, 29 FR 17955, Dec. 18, 1964, as amended by Amdt. 23-7, 34 FR 13090, Aug. 13, 1969; Amdt. 23-28, 47 FR 13315, Mar. 29, 1982; Amdt. 23-45, 58 FR 42160, Aug. 6, 1993; Amdt. 23-48, 61 FR 5147, Feb. 9, 1996]

§23.477 Landing gear arrangement.

Sections 23.479 through 23.483, or the conditions in appendix C, apply to airplanes with conventional arrangements

EMBRY-RIDDLE AERONAUTICAL UNIVERSITY

A.05 - Side loads conditions and assumptions.

of main and nose gear, or main and tail gear.

§ 23.479 Level landing conditions.

(a) For a level landing, the airplane is assumed to be in the following attitudes:

(1) For airplanes with tail wheels, a normal level flight attitude.

(2) For airplanes with nose wheels, attitudes in which—

(i) The nose and main wheels contact the ground simultaneously; and

(ii) The main wheels contact the ground and the nose wheel is just clear of the ground.

The attitude used in paragraph (a)(2)(i) of this section may be used in the analysis required under paragraph (a)(2)(ii) of this section.

(b) When investigating landing conditions, the drag components simulating the forces required to accelerate the tires and wheels up to the landing speed (spin-up) must be properly combined with the corresponding instantaneous vertical ground reactions, and the forward-acting horizontal loads resulting from rapid reduction of the spin-up drag loads (spring-back) must be combined with vertical ground reactions at the instant of the peak forward load, assuming wing lift and a tire-sliding coefficient of friction of 0.8. However, the drag loads may not be less than 25 percent of the maximum vertical ground reactions (neglecting wing lift).

(c) In the absence of specific tests or a more rational analysis for determining the wheel spin-up and spring-back loads for landing conditions, the method set forth in appendix D of this part must be used. If appendix D of this part is used, the drag components used for design must not be less than those given by appendix C of this part.

(d) For airplanes with tip tanks or large overhung masses (such as turbopropeller or jet engines) supported by the wing, the tip tanks and the structure supporting the tanks or overhung masses must be designed for the effects of dynamic responses under the level landing conditions of either paragraph (a)(1) or (a)(2)(ii) of this section. In evaluating the effects of dynamic response, an airplane lift equal to the weight of the airplane may be assumed.

[Doc. No. 4080, 29 FR 17955, Dec. 18, 1964, as amended by Amdt. 23–17, 41 FR 55464, Dec. 20, 1976; Amdt. 23–45, 58 FR 42160, Aug. 6, 1993]

§ 23.481 Tail down landing conditions.

(a) For a tail down landing, the airplane is assumed to be in the following attitudes:

(1) For airplanes with tail wheels, an attitude in which the main and tail wheels contact the ground simultaneously.

(2) For airplanes with nose wheels, a stalling attitude, or the maximum angle allowing ground clearance by each part of the airplane, whichever is less.

(b) For airplanes with either tail or nose wheels, ground reactions are assumed to be vertical, with the wheels up to speed before the maximum vertical load is attained.

§ 23.483 One-wheel landing conditions.

For the one-wheel landing condition, the airplane is assumed to be in the level attitude and to contact the ground on one side of the main landing gear. In this attitude, the ground reactions must be the same as those obtained on that side under § 23.479.

§ 23.485 Side load conditions.

(a) For the side load condition, the airplane is assumed to be in a level attitude with only the main wheels contacting the ground and with the shock absorbers and tires in their static positions.

(b) The limit vertical load factor must be 1.33, with the vertical ground reaction divided equally between the main wheels.

(c) The limit side inertia factor must be 0.83, with the side ground reaction divided between the main wheels so that—

(1) 0.5 (*W*) is acting inboard on one side; and

(2) 0.33 (*W*) is acting outboard on the other side.

(d) The side loads prescribed in paragraph (c) of this section are assumed to be applied at the ground contact point

A.06 - Ground load unsymmetrical loads on multiple-wheel units.

§ 23.511 Ground load; unsymmetrical loads on multiple-wheel units.

(a) *Pivoting loads.* The airplane is assumed to pivot about on side of the main gear with—

(1) The brakes on the pivoting unit locked; and

(2) Loads corresponding to a limit vertical load factor of 1, and coefficient of friction of 0.8 applied to the main gear and its supporting structure.

(b) *Unequal tire loads.* The loads established under §§ 23.471 through 23.483 must be applied in turn, in a 60/40 percent distribution, to the dual wheels and tires in each dual wheel landing gear unit.

(c) *Deflated tire loads.* For the deflated tire condition—

(1) 60 percent of the loads established under §§ 23.471 through 23.483 must be applied in turn to each wheel in a landing gear unit; and

(2) 60 percent of the limit drag and side loads, and 100 percent of the limit vertical load established under §§ 23.485 and 23.493 or lesser vertical load obtained under paragraph (c)(1) of this section, must be applied in turn to each wheel in the dual wheel landing gear unit.

[Amdt. 23-7, 34 FR 13090, Aug. 13, 1969]

WATER LOADS

A.07 - Airspeed limits of Utility and Aerobatic Bonanza.

Model F33C, Bonanza, 2 PCLM (Acrobatic Category), approved October 24, 1969

Engine	Continental IO-520-B or IO-520-BA; IO-520-BB (CE-816 and up, CJ-149 and up) *See Item 120 for optional engine.*			
*Fuel	Aviation gasoline Grade 100LL or 100 minimum			
*Engine Limits	(For all airplanes prior to CE-891 and CJ-156 and airplanes CE-891 and after and CJ-156 and after equipped with Item 14(a) or 18(a)) For all operations 2700 rpm (285 hp) (For airplanes CE-891 and after and CJ-156 and after equipped with Item 11(a)) Takeoff and continuous power 2700 rpm (285 hp) Normal operating power 2550 rpm (275 hp)			
*Airspeed Limits	Utility Category (F33A, F33C)	CAS	CAS	IAS
	Maneuvering	152 mph	(132 knots)	(134 knots)
	Maximum structural cruising	190 mph	(165 knots)	(167 knots)
	Never exceed	225 mph	(195 knots)	(197 knots)
	Flaps extended (15°) (S/N's CE-816 and after) (S/N's CJ-150 and after)	175 mph	(152 knots)	(154 knots)
	Flaps extended (normal)	140 mph	(122 knots)	(123 knots)
	Landing gear extended (normal)	175 mph	(152 knots)	(154 knots)
	Acrobatic Category (F33C)	CAS	CAS	IAS
	Maneuvering	165 mph	(143 knots)	(145 knots)
	Maximum structural cruising	190 mph	(165 knots)	(167 knots)
	Never exceed	234 mph	(203 knots)	(204 knots)
	Flaps extended (12°) (S/N's CJ-150 and after)	175 mph	(152 knots)	(154 knots)
	Flaps extended (normal)	140 mph	(122 knots)	(123 knots)
	Landing gear extended (normal)	175 mph	(152 knots)	(154 knots)

A.08 - Simplified version of moment calculation on wing.

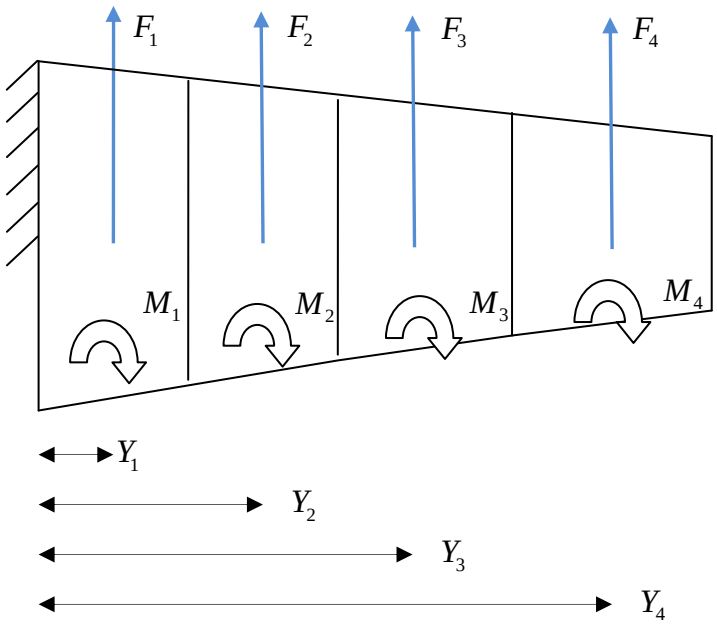

$$M_4 = 0$$
$$M_3 = F_4 \cdot (Y_4 - Y_3)$$
$$M_2 = F_4 \cdot (Y_4 - Y_2) + F_3 \cdot (Y_3 - Y_2)$$
$$M_1 = F_4 \cdot (Y_4 - Y_1) + F_3 \cdot (Y_3 - Y_1) + F_2 \cdot (Y_2 - Y_1)$$

A.09 – Detailed explanation on procedure to get loads.

From the type certificate data sheet from the FAA, the values of the CG range were found to be: (+78.5) to (+81) for acrobatic aircraft that weights 2800lbs. The datum for such range is taken 83.1 inches forward of jack pads on front spars. From approximations in the scale drawings the datum is believed to be just behind the propeller.

Dimensions are taken from a scale drawing of a Beechcraft Bonanza F33C.

The approximated dimensions taken were:

Distance from right main gear to left main gear: 9.45 ft
Height from ground to cg approximately: 3.15ft
Distance from datum to nose gear: 0ft
Distance from datum to main gear: 7 ft

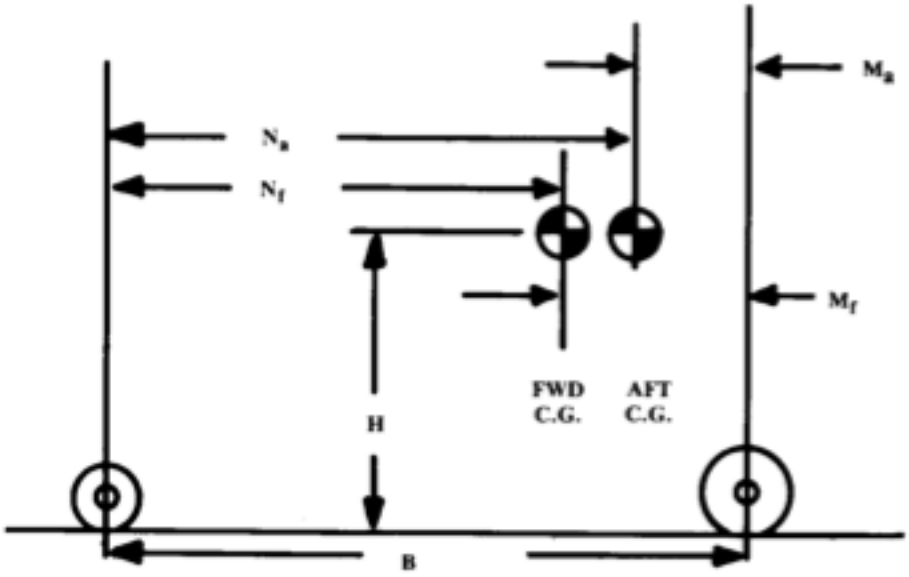

Figure 1: Wheel load Geometry (Raymer 234)

This picture references the distances:

B= 7 ft
Nf = 78.5 in = 6.54ft
Na= 81in = 6.75 ft
Ma= 1.125ft
Mf= 1.335ft
H= 3.15ft

With these dimensions and the following formulas also taken from Raymer's book

$$(\text{Max Static Load}) = W\frac{N_a}{B} \qquad (11.1)$$

$$(\text{Max Static Load})_{nose} = W\frac{M_f}{B} \qquad (11.2)$$

$$(\text{Min Static Load})_{nose} = W\frac{M_a}{B} \qquad (11.3)$$

$$(\text{Dynamic Braking Load})_{nose} = \frac{10HW}{gB} \qquad (11.4)$$

Figure 2: Load formulas (Raymer 234)

Refering to FAR section 23.499 nose wheel loads are applied as follows:

For aft loads, limit loads at axle must be able to withstand:
Vertical component of 2.25 times the static load on the nose wheel.
A drag component of 0.8 times the vertical load.

For forward loads:
Vertical component of 2.25 times the static load on the nose wheel
A forward component of 0.4 times the vertical load.

For side loads, the limit force components at the ground contact must be:
Vertical component of 2.25 times the static load on the nose wheel.
A side component of 0.7 times the vertical load.

For Main Gear Loads Calculations:
The landing impact loads depend on the landing contact velocity. To calculate that velocity according to FAR section 23.473 use the following formula:

—

The inertia load factor is based (in this case) only on the FAR.

The inertia load factor due to the landing impact is unknown, but is chosen to be 3.0 until the actual value is obtained.

The force applied on each wheel is the weight of the aircraft times the inertia load factor divided by 2 (because there are 2 main gear).

The side force is also found according to FAR part 23.511 by multiplying the weight times a side inertia factor of 0.83. The ground reaction is also taken into consideration; this is divided between the main wheels so that half of the weight is acting inboard and 0.33 times the weight is acting outboard. The drag reaction is accounted for as well. According to the FAA section 23.499 regulations a coefficient of friction of 0.8 has to be multiplied by the vertical reaction (vertical force applied on each wheel)

A.10 – Differences between CAR's and FAR's for the landing gear loads

Civil Aviation Regulations CAR's

§ 3.243 *Load factor for landing conditions.* In the following landing conditions the limit vertical inertia load factor at the center of gravity of the airplane shall be chosen by the designer but shall not be less than the value which would be obtained when landing the airplane with a descent velocity, in feet per second, equal to the following value:

$$V = 4.4\ (W/S)^{1/4}$$

except that the descent velocity need not exceed 10 feet per second and shall not be less than 7 feet per second.

… In no case, however, shall the inertia load factor used for design purposes be less than 2.67, nor shall the limit ground reaction load factor be less than 2.0, unless it is demonstrated that lower values of limit load factor will not be exceeded in taxiing the airplane over terrain having the maximum degree of roughness to be expected under intended service use at all speeds up to take-off speed.

Condition	Nose wheel type		
	Level landing with inclined reactions	Level landing with nose wheel just clear of ground	Tail-down landing
Reference section----	§ 3.245 (b) (1)	§ 3.245 (b) (2)	§ 3.246 (b) (c)
Vertical component at c.g.----------	nW	nW	nW
Fore and aft component at c.g.----------	KnW	KnW	0
Lateral component in either direction at c.g.	0	0	0
Shock absorber extension (hydraulic shock absorber)------	Note (2)	Note (2)	Note (2)
Shock absorber deflection (rubber or spring shock absorber)----------	100% Static	100% Static	100% Static
Tire deflection----------			
Main wheel loads (both wheels)----------{	nWb'/d'	nW	nW
{D,	K_{V_s}	K_{V_s}	0
Tail (nose) wheel loads ----------{	nWa'/d'	0	0
{D,	K_{V_t}	0	0
Notes----------	(1)	(1) and (3)	(3)

Note (1).—K may be determined as follows: K=0.25 for W=3,000 pounds or less; K=0.33 for W=6,000 pounds or greater with linear variation of K between these weights.

Note (2).—For the purpose of design, the maximum load factor shall be assumed to occur throughout the shock absorber stroke from 25 percent deflection to 100 percent deflection unless demonstrated otherwise, and the load factor shall be used with whatever shock absorber extension is most critical for each element of the landing gear.

Note (3).—Unbalanced moments shall be balanced by a rational or conservative method.

Federal Aviation Regulations FAR's

§ 23.485 Side load conditions.

(a) For the side load condition, the airplane is assumed to be in a level attitude with only the main wheels contacting the ground and with the shock absorbers and tires in their static positions.

(b) The limit vertical load factor must be 1.33, with the vertical ground reaction divided equally between the main wheels.

(c) The limit side inertia factor must be 0.83, with the side ground reaction divided between the main wheels so that—

(1) 0.5 (W) is acting inboard on one side; and

(2) 0.33 (W) is acting outboard on the other side.

Section **§ 23.499 Supplementary conditions for nose wheels.** Is comparable with section § 3.253 *Supplementary conditions for nose wheels.* Everything is the same except that FAR's have the following:

(d) For airplanes with a steerable nose wheel that is controlled by hydraulic or other power, at design takeoff weight with the nose wheel in any steerable position, the application of

1.33 times the full steering torque combined with a vertical reaction equal to

1.33 times the maximum static reaction on the nose gear must be assumed. However, if a torque limiting device is installed, the steering torque can be reduced to the maximum value allowed by that device.

(e) For airplanes with a steerable nose wheel that has a direct mechanical connection to the rudder pedals, the mechanism must be designed to withstand the steering torque for the maximum pilot forces specified in § 23.397(b).

A.11 Differences between CAR's and FAR's for the air loads and flight envelope

From CAR:

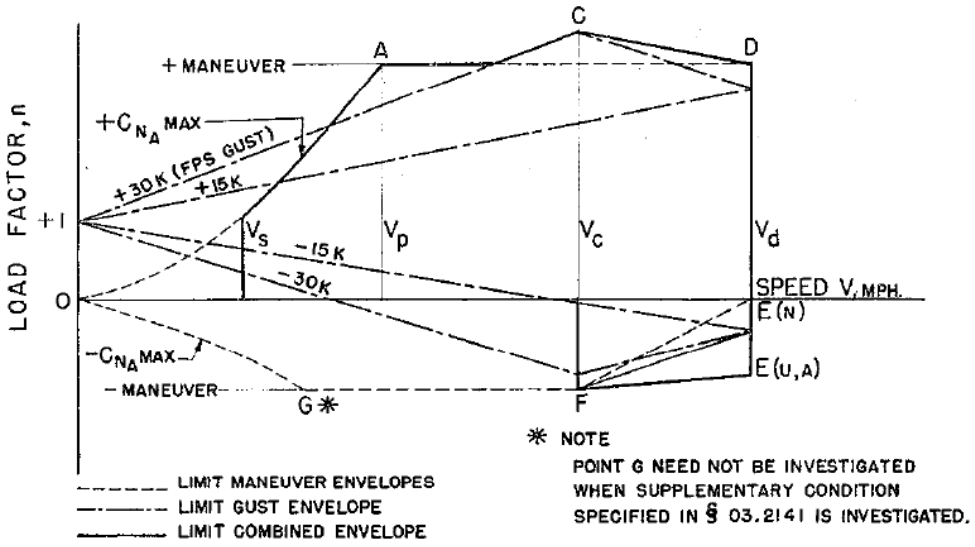

FIG. 03-1—(V-n) DIAGRAM (FLIGHT ENVELOPE)

13

03.2110 Design air speeds. The design air speeds shall be chosen by the designer except that they shall not be less than the following values:

V_c (design cruising speed)

$= 38\sqrt{W/S}$ (NU)

$= 42\sqrt{W/S}$ (A)

except that for values of W/S greater than 20, the above numerical multiplying factors shall be decreased linearly with W/S to a value of 33 at $W/S = 100$, and further provided, that the required minimum value need be no greater than $0.9V_h$ actually obtained at sea level.

V_d (design dive speed)

$= 1.40\ V_{c_{min}}$ (N)

$= 1.50\ V_{c_{min}}$ (U)

$= 1.55\ V_{c_{min}}$ (A)

except that for values of W/S greater than 20, the above numerical multiplying factors shall be decreased linearly with W/S to a value of 1.35 at $W/S = 100$. ($V_{c_{min}}$ is the required minimum value of design cruising speed specified above.)

V_p (design maneuvering speed)

$= V_s\sqrt{n}$ where:

V_s = a computed stalling speed with flaps fully retracted at the design weight, normally based on the maximum airplane normal force coefficient C_{N_A},

n = limit maneuvering load factor used in design,

except that the value of V_p need not exceed the value of V_c used in design.

03.21120 Gust load factors. In applying the gust requirements, the gust load factors shall be computed by the following formula:

$$n = 1 + \frac{K\,U\,V\,m}{575\,(W/S)}$$

where: $K = \frac{1}{2}(W/S)^{1/4}$ (for $W/S < 16$ psf)

$$= 1.33 - \frac{2.67}{(W/S)^{3/4}} \quad \text{(for } W/S > 16 \text{ psf)}$$

U = nominal gust velocity, fps. (Note that the "effective sharp-edged gust" equals KU)
V = airplane speed, mph
m = slope of lift curve, C_L per radian, corrected for aspect ratio
W/S = wing loading, psf

03.2113 Airplane equilibrium. In determining the wing loads and linear inertia loads corresponding to any of the above specified flight conditions, the appropriate balancing horizontal tail load (see § 03.2211) shall be taken into account in a rational or conservative manner.

Incremental horizontal tail loads due to maneuvering and gusts (see §§ 03.2212 and 03.2213) shall be reacted by angular inertia of the complete airplane in a rational or conservative manner.

03.212 Flaps extended flight conditions. When flaps or similar high lift devices intended for use at the relatively low air speeds of approach, landing, and take-off are installed, the airplane shall be assumed to be subjected to symmetrical maneuvers and gusts with the flaps fully deflected at the design flap speed V_f resulting in limit load factors within the range determined by the following conditions:

(a) maneuvering, to a positive limit load factor of 2.0,

(b) positive and negative 15 fps gusts acting normal to the flight path in level flight. The gust load factors shall be computed by the formula of § 03.21120.

V_f shall be assumed not less than 1.4 V_s or 1.8 V_{sf}, whichever is greater, where:

V_s = the computed stalling speed with flaps fully retracted at the design weight,
V_{sf} = the computed stalling speed with flaps fully extended at the design weight,

except that, when an automatic flap load limiting device is employed, the airplane may be designed for critical combinations of air speed and flap position permitted by the device. (See also § 03.353.)

In designing the flaps and supporting structure, slipstream effects shall be taken into account as specified in § 03.224.

NOTE: In determining the external loads on the airplane as a whole, the thrust, slipstream, and pitching acceleration may be assumed equal to zero.

From FAR:

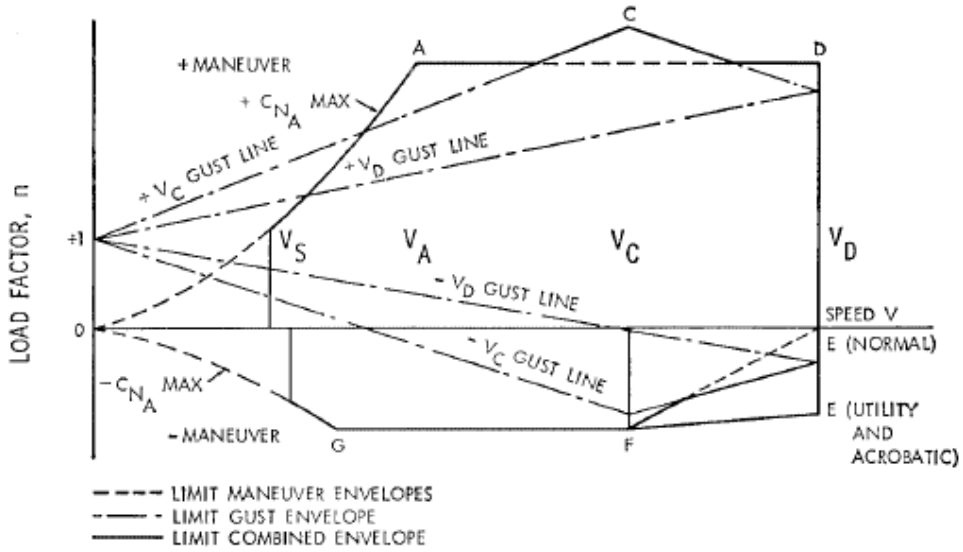

[Doc. No. 4080, 29 FR 17955, Dec. 18, 1964, as amended by Amdt. 23-7, 34 FR 13087, Aug. 13, 1969; Amdt. 23-34, 52 FR 1829, Jan. 15, 1987]

§ 23.335 Design airspeeds.

Except as provided in paragraph (a)(4) of this section, the selected design airspeeds are equivalent airspeeds (EAS).

(a) *Design cruising speed, V_C.* For V_C the following apply:

(1) Where W/S'=wing loading at the design maximum takeoff weight, V_c (in knots) may not be less than—

(i) 33 $\sqrt{(W/S)}$ (for normal, utility, and commuter category airplanes);

(ii) 36 $\sqrt{(W/S)}$ (for acrobatic category airplanes).

(2) For values of *W/S* more than 20, the multiplying factors may be decreased linearly with *W/S* to a value of 28.6 where *W/S*=100.

(3) V_C need not be more than 0.9 V_H at sea level.

(4) At altitudes where an M_D is established, a cruising speed M_C limited by compressibility may be selected.

(b) *Design dive speed V_D.* For V_D the following apply:

(1) V_D/M_D may not be less than 1.25 V_C/M_C; and

(2) With $V_{C\ min}$ the required minimum design cruising speed, V_D (in knots) may not be less than—

(i) 1.40 $V_{c\ min}$ (for normal and commuter category airplanes);

(ii) 1.50 $V_{C\ min}$ (for utility category airplanes); and

(iii) 1.55 $V_{C\ min}$ (for acrobatic category airplanes).

(3) For values of *W/S* more than 20, the multiplying factors in paragraph (b)(2) of this section may be decreased linearly with *W/S* to a value of 1.35 where *W/S*=100.

(4) Compliance with paragraphs (b)(1) and (2) of this section need not be shown if V_D/M_D is selected so that the minimum speed margin between V_C/M_C and V_D/M_D is the greater of the following:

(i) The speed increase resulting when, from the initial condition of stabilized flight at V_C/M_C, the airplane is assumed to be upset, flown for 20 seconds along a flight path 7.5° below the initial path, and then pulled up with a load factor of 1.5 (0.5 *g.* acceleration increment). At least 75 percent maximum continuous power for reciprocating engines, and maximum cruising power for turbines, or, if less, the power required for V_C/M_C for both kinds of engines, must be assumed until the pullup is initiated, at which point power reduction and pilot-controlled drag devices may be used; and either—

(ii) Mach 0.05 for normal, utility, and acrobatic category airplanes (at altitudes where M_D is established); or

(iii) Mach 0.07 for commuter category airplanes (at altitudes where M_D is established) unless a rational analysis, including the effects of automatic systems, is used to determine a lower margin. If a rational analysis is used, the minimum speed margin must be enough to provide for atmospheric variations (such as horizontal gusts), and the penetration of jet streams or cold fronts), instrument errors, airframe production variations, and must not be less than Mach 0.05.

(c) *Design maneuvering speed* V_A. For V_A the following applies:

(1) V_A may not be less than $V_S\sqrt{n}$ where—

(i) V_S is a computed stalling speed with flaps retracted at the design weight, normally based on the maximum airplane normal force coefficients, C_{NA}; and

(ii) n is the limit maneuvering load factor used in design

(2) The value of V_A need not exceed the value of V_C used in design.

(d) *Design speed for maximum gust intensity, V_B.* For V_B, the following apply:

(1) V_B may not be less than the speed determined by the intersection of the line representing the maximum positive lift, C_{NMAX}, and the line representing the rough air gust velocity on the gust V-n diagram, or $V_{S1}\sqrt{n_g}$, whichever is less, where:

(i) n_g the positive airplane gust load factor due to gust, at speed V_C (in accordance with §23.341), and at the particular weight under consideration; and

(ii) V_{S1} is the stalling speed with the flaps retracted at the particular weight under consideration.

(2) V_B need not be greater than V_C.

[Doc. No. 4080, 29 FR 17955, Dec. 18, 1964, as amended by Amdt. 23–7, 34 FR 13088, Aug. 13, 1969; Amdt. 23–16, 40 FR 2577, Jan. 14, 1975; Amdt. 23–34, 52 FR 1829, Jan. 15, 1987; Amdt. 23–24, 52 FR 34745, Sept. 14, 1987; Amdt. 23–48, 61 FR 5143, Feb. 9, 1996]

§23.337 Limit maneuvering load factors.

(a) The positive limit maneuvering load factor n may not be less than—

(1) 2.1+(24,000+(W+10,000)) for normal and commuter category airplanes, where W=design maximum takeoff weight, except that n need not be more than 3.8;

(2) 4.4 for utility category airplanes; or

(3) 6.0 for acrobatic category airplanes.

(b) The negative limit maneuvering load factor may not be less than—

(1) 0.4 times the positive load factor for the normal utility and commuter categories; or

(2) 0.5 times the positive load factor for the acrobatic category.

(c) Maneuvering load factors lower than those specified in this section may be used if the airplane has design features that make it impossible to exceed these values in flight.

[Doc. No. 4080, 29 FR 17955, Dec. 18, 1964, as amended by Amdt. 23–7, 34 FR 13088, Aug. 13, 1969; Amdt. 23–34, 52 FR 1829, Jan. 15, 1987; Amdt. 23–48, 61 FR 5144, Feb. 9, 1996]

§23.341 Gust loads factors.

(a) Each airplane must be designed to withstand loads on each lifting surface resulting from gusts specified in §23.333(c).

(b) The gust load for a canard or tandem wing configuration must be computed using a rational analysis, or may be computed in accordance with paragraph (c) of this section, provided that the resulting net loads are shown to be conservative with respect to the gust criteria of §23.333(c).

(c) In the absence of a more rational analysis, the gust load factors must be computed as follows—

$$n = 1 + \frac{K_g U_{de} V a}{498\,(W/S)}$$

Where—

K_g=0.88μ_g/5.3+μ_g=gust alleviation factor;

μ_g=2(W/S)/ρ Cag=airplane mass ratio;

U_{de}=Derived gust velocities referred to in §23.333(c) (f.p.s.);

ρ=Density of air (slugs/cu.ft.);

W/S=Wing loading (p.s.f.) due to the applicable weight of the airplane in the particular load case.

W/S=Wing loading (p.s.f.);

C=Mean geometric chord (ft.);

g=Acceleration due to gravity (ft./sec.^{2})

V=Airplane equivalent speed (knots); and

a=Slope of the airplane normal force coefficient curve C_{NA} per radian if the gust loads are applied to the wings and horizontal tail

References:
Civil Aviation Regulations Subpart 3
Federal Aviation Regulations Subpart 23
Raymer, Daniel. *Aircraft Design: A Conceptual Approach*. Washington D.C.: American Institute of Aeronautics and Astronautics, 1992. 234. Print.